Laser polishing and structuring by laser remelting of 1.2379+

Of

Magdalena Cortina Burón

Master thesis in Mechanical Engineering

Submitted to

Faculty of Mechanical Engineering

of Rheinisch-Westfälische Technische Hochschule Aachen

at 30/07/2016

composed at

Chair for Laser Technology

Prof. Dr. rer. nat. R. Poprawe M. A.

Contents

1 Introduction & Objective

Extrusion is a forming process with great versatility and a wide spectrum of industrial applications, ranging from the household sector to the automotive, aerospace or oil & gas among others [1]. Cold extrusion processes are well known because of the dimensional accuracy of the formed parts, as well as their high surface quality and improvements in mechanical properties [2]. One of the main drawbacks in cold extrusion of aluminum is the adhesion wear mechanism that happens between the extrusion die and the extruded material. In order to prevent this effect excessive usage of lubrication is necessary, leading to subsequent cleaning steps and entailing economic and ecological issues. Thus, the development of new dry metal forming processes so that a lubricant-free status is accomplished is highly desirable. Vollertsen et al. define dry metal forming as a "process where a workpiece leaves the forming tool without the necessity of cleaning or drying before further production steps" [3]. The absence of lubricant involves an intense wear behavior due to the interaction between extrusion die and work piece, that needs to be relieved. New strategies to achieve an improved wear behavior involve the development of modifications for the tools and work pieces respectively.

In the project "Schmiermittelfreie Tribologiekonzepte für das Kaltfließpressen durch interaktionsminimierte Oberflächenschichten und -strukturen", funded by the Deutsche Forschungsgemeinschaft within the priority program 1676, laser polishing and structuring by laser remelting processes are developed and the influence of these surface modifications on the adhesive wear behavior of 1.2379+ cold work steel is investigated. The basis for this will be the definition of process parameters for laser polishing and structuring by remelting as well as the characterization of the produced surfaces. On the one hand, by using macro polishing with continuous wave as well as micro polishing with pulsed laser radiation different spatial wavelengths ranges of the surface roughness are modified. On the other hand, by structuring by remelting the surface of the work tool is structured without removing any material, but redistributing it while molten.

The objective of this work is the development of the laser polishing and structuring by remelting processes for 1.2379+ and to analyze which wavelengths of the roughness spectrum are influenced by which process and corresponding process parameters.

2 State of the Art

2.1 Laser polishing fundamentals

Laser polishing of metallic surfaces is an emerging manufacturing process that is regarded to replace the expensive and time-consuming manual polishing operations. Furthermore, manual polishing results depend to a great extent on the skills and condition of the worker, whereas laser polishing is completely suitable for automation.

During laser polishing a thin surface layer is molten by laser radiation forming a melt pool. Along this phenomena, material flows from the peaks to the valleys due to surface tension and the structures with a spatial wavelength which is smaller than the laser beam diameter resolidify smoothed. Hence, the innovation of this process compared to conventional polishing is that there is no ablation, material is not removed but redistributed while melted.

Laser polishing of an area is achieved by scanning the laser spot in a meander pattern over the surface. In Figure 1 a scheme of the process fundamentals and main process parameters is shown.

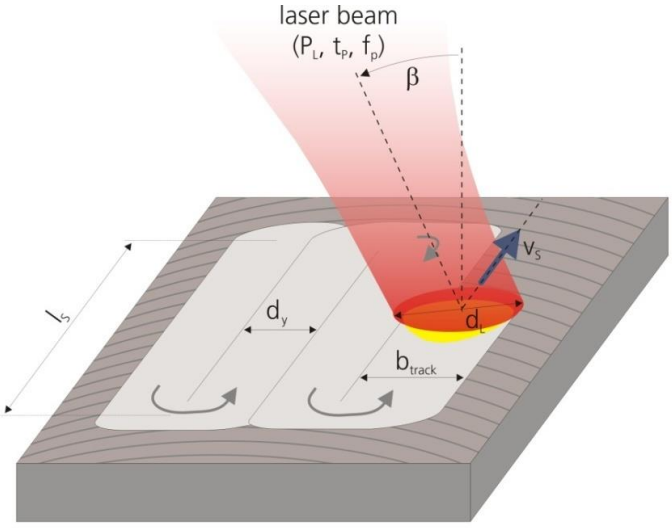

Figure 1: Scheme of process fundamentals for laser polishing [14]

The main process parameters are: laser power P_L, pulse duration t_p, frequency of repetition f_p, spot size d_L, scan velocity v_{scan}, track offset dy, scan vector length l_s, width of track b_{track}, angle of incidence β.

There are two different process variants: macro and micro polishing, which are based on operating with continuous wave (cw) and pulsed laser radiation, respectively. As far as macro polishing is concerned, a continuous melt pool (see Figure 2 - a) with a melting depth typically ranging from 20 to 100 µm is created [4][5], smoothening areas with an initial roughness of Ra = 1.0 µm or higher, e.g. after milling, turning or EDM-processing. Alternatively, micro polishing is based on a discrete remelting process where each melt pool resolidifies when the pulsed radiation hits and creates a new one, as it can be appreciated in Figure 2 - b. This variant is a combination of remelting a thin surface layer (less than 5 µm depth) [4][5] and micro peaks vaporization, so that it is applied to fine pre-processed surfaces with Ra = 0.8 µm or lower, leaving bigger structures unaffected.

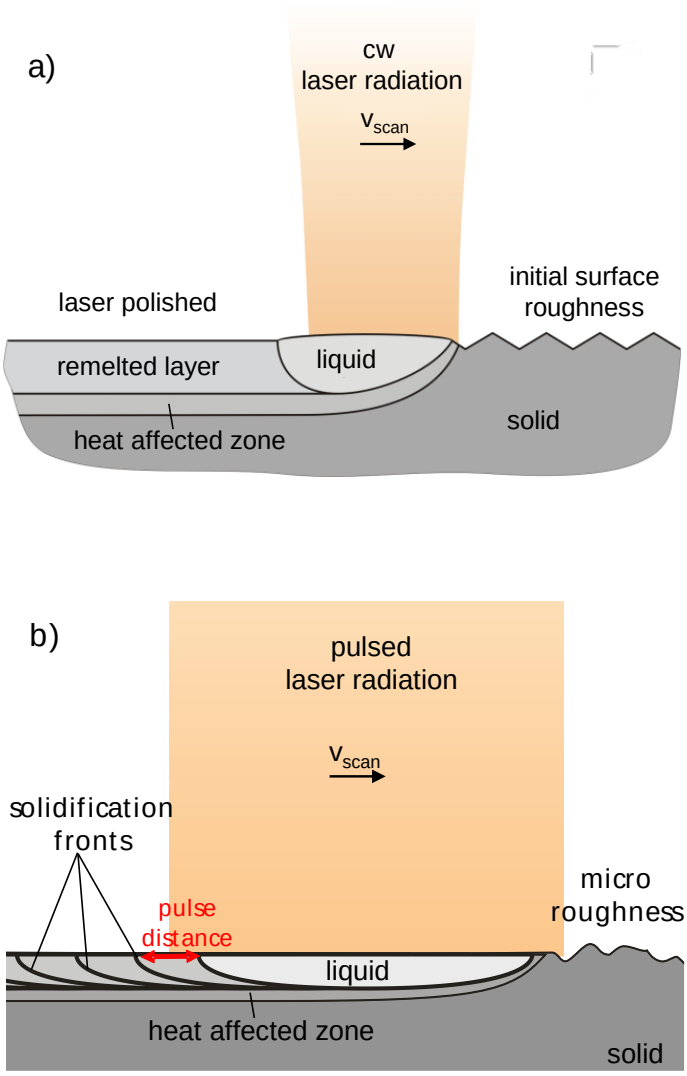

Figure 2:
Scheme of process principles.
a) Macro polishing with cw radiation
b) Micro polishing with pulsed radiation
[14]

Laser beam diameters for polishing usually range from 125 - 600 µm, affecting surface's spatial wavelengths within this range and leaving waviness intact. Surface waviness can be created, modified or erased using structuring by laser remelting.

2.2 Structuring by laser remelting fundamentals

Surface structuring manufacturing processes are traditionally based on material removal, e.g. photochemical etching or structuring by laser ablation. Therefore, cleaning and finishing steps are required with the consequent economic implications. Structuring by laser remelting is a new approach based on the redistribution of material while molten, refraining from material loss, with the subsequent advantages: economic saving and no necessity of finishing operations. The latter is due to the smoothening of the surface that happens during the structuring process.

Structuring by remelting modifies the surface of metals by the modulation of the melt pool. This modulation can be achieved by means of varying laser power so that a new surface topography determined by the movement of the three-phase point is obtained.

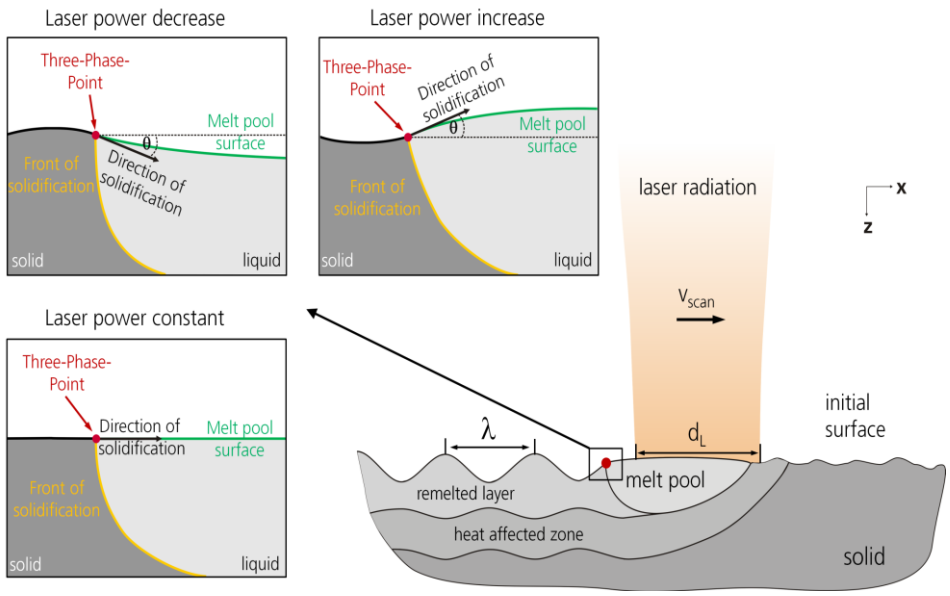

Figure 3: Schematic of active principle for structuring by laser remelting [15]

The principle of structuring by laser remelting is shown in Figure 3, where a thin surface layer (< 100 µm depth) is molten at the melt front (on the right), and then

solidifies at the solidification front (on the left) following the melt pool's surface. Actual solidification takes place at the three-phase point, which is highlighted in the figure. Thus, when laser power is constant the surface of the melt pool is practically flat and there is no structuring. However, when laser power is increased and decreased the volume of the pool varies and structuring happens. Then, increasing laser power implies a rise of the melt pool volume due to the density change from solid to liquid, thermal dilatation of the molten material and a higher melt rate compared to the solidification rate. As a result, the melt pool surface is bulged outwards and the structuring of an elevation is achieved. Alternatively, decreasing power leads to a contraction of the melt pool and works the other way around, attaining the structuring of a dip. Hence, by remelting a thin surface layer while modulating laser power, structuring without ablation can be achieved.

The final surface topography depends on how power is modulated. In order to obtain periodic structures, laser power is modulated sinusoidally (see Figure 4). For that purpose, the upper and lower limits of laser power need to be determined, being $P_{L\ melt}$ the minimum laser power required in order to start remelting and have a stable melt pool and $P_{L\ evap.}$ the maximum laser power after which material starts to evaporate.

Figure 4: Schematic of laser power modulation parameters [15]

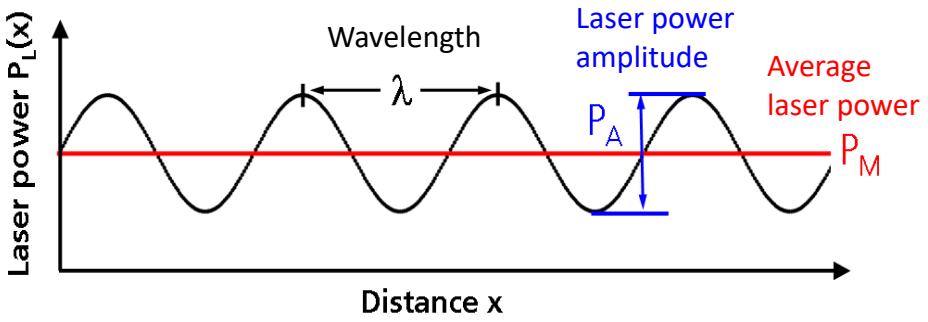

The range of power $P_{L\ melt}$ - $P_{L\ evap.}$ consequently defines both average laser power P_M and laser power amplitude P_A. On the one hand, the average laser power P_M is defined as

2.1

$$P_M = \frac{P_{L\ evap.} + P_{L\ melt}}{2}$$

On the other hand, the laser power amplitude is determined by

2.2

$$P_A = \frac{P_{L\ evap.} - P_{L\ melt}}{2}$$

While laser power is modulated, the laser beam with diameter d_L is guided unidirectionally over the surface with a definite scan velocity, v_{scan}, and track offset, dy, as shown in Figure 5.

Figure 5: Schematic of the process [15]

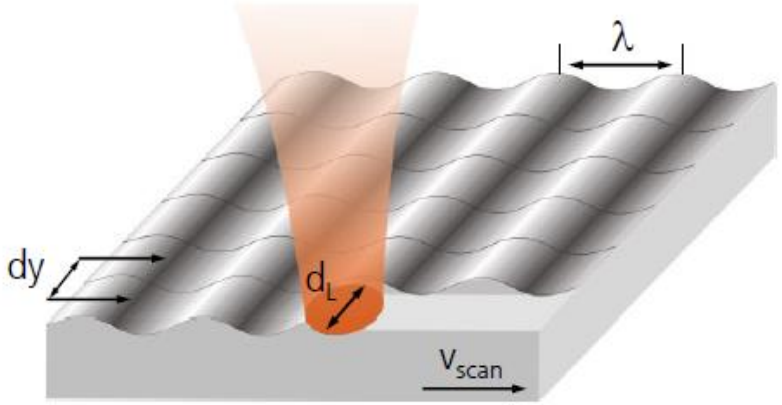

The most relevant parameters for the remelting process are, the average laser power, the laser power amplitude, the wavelength of the modulation, the scanning velocity and the size or diameter of the laser beam. Therefore, the process can be conducted and automated by means of software programs, which is important for industrial purposes.

3 Experimental set-up

3.1 Machine Technology

As part of a publicly funded project, Fraunhofer Institute for Laser Technology (ILT) in cooperation with Maschinenfabrik Arnold developed the "POLAR" prototype laser polishing machine. All experiments described in this thesis are performed on this machine, employs five mechanical axes (three linear and two rotatory) for positioning the work piece relative to the laser beam combined with a HurryScan25 and VarioScan40, a galvanometer scanner by Scanlab which deflects the laser beam onto the work piece's surface. Therefore, this is a five mechanical plus three "optical" axes machine whose work piece capacity regarding size and weight is ∅ 280x250 mm³ / 200 kg.

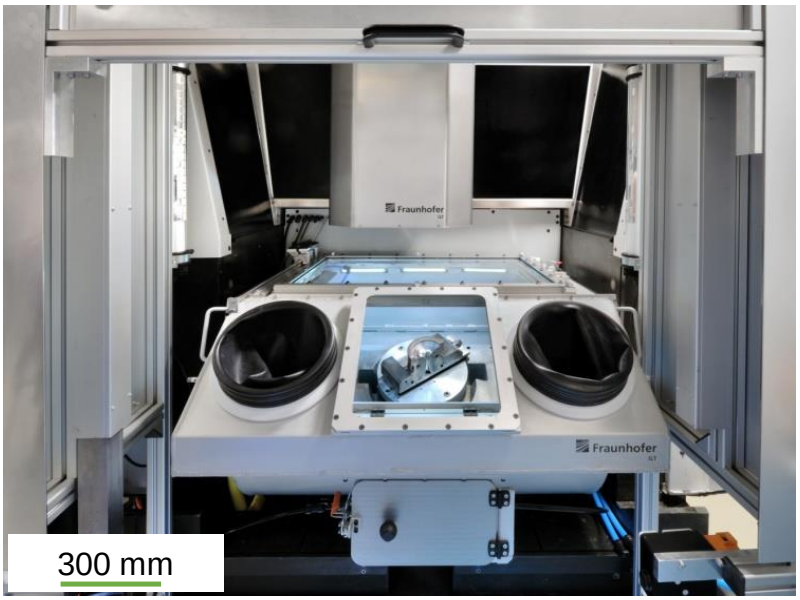

Figure 6: Photograph of "POLAR" machine

In this thesis, two different Yb:YAG, solid-state disc laser sources supplied by TRUMPF are used. For micro polishing, a fiber-coupled, Q-switched TruMicro 7051 laser is used. The maximum power output of this is $P_{L\,max}$ = 500 W with an emitting wavelength λ_{em} = 1030 nm, repetition frequency f_p = 5 - 20 kHz and pulse duration t_p ~ 1 µs (@ $P_{L,max}$). For macro polishing and structuring by remelting, a TruDisk 1000 continuous wave laser is utilized, with $P_{L\,max}$ = 1000 W and λ_{em} = 1030 nm.

The laser systems are connected to the machine's processing optic by a Trumpf laser light cable with a square 100x100 µm² core fiber. The processing optic includes a

power attenuator, used for controlling the process laser power in combination with the TruMicro, a motorized zoom telescope, which allows the change of the laser spot size, the Scanlab galvanometer scanner and a f-theta lens. Aiming to reduce unwanted oxidations during the process, the investigations take place in a process chamber filled with Argon. The residual oxygen is monitored and adjusted by a closed-loop control.

3.2 Laser beam characteristics

All experimental investigations are performed with a square 100x100µm² fiber. Since different spot sizes (100x100, 200x200 and 400x400 µm²) are used, various tools need to be defined for each size and laser source employed. The relevant parameters for defining the tools are zoom position, attenuation angle (necessary for the power attenuator of the TruMicro), z offset and individual power curves.

The zoom position is determined by analyzing the caustic beam and the attenuation angle and power curves by carrying out laser power measurements. In order to determine the focus position, meander patterns are marked on a flat aluminum plate at different z-positions.

3.2.1 Caustic beam measurement

The zoom position is obtained by selecting the one which ensures the required spot size and intensity distribution. MicroSpotMonitor (MSM) by Primes is used for analyzing the caustic and determining that parameter. This device determines beam parameters of focused laser beams with average laser powers up to 200 W in the range from 20 - 1000 µm. [10]

The MSM is placed under the f-theta lens to measure and analyze the spatial beam distribution all around the focus on several planes at different z positions, so that the complete caustic beam is obtained. Then, the results are processed with LaserDiagnoseSoftware v2.98 by Primes, which allows to measure the energy distributions. Thus, the planes with the desired intensity distribution and laser spot size are identified at the focus position, obtaining the zoom positions for each tool size, as it can be observed in Figure 7.

Figure 7:
Intensity distribution laser spot sizes of the employed tools:

a) 100x100 µm²
Zoom 0
b) 200x200 µm²
Zoom 16
c) 400x400 µm²
Zoom 32

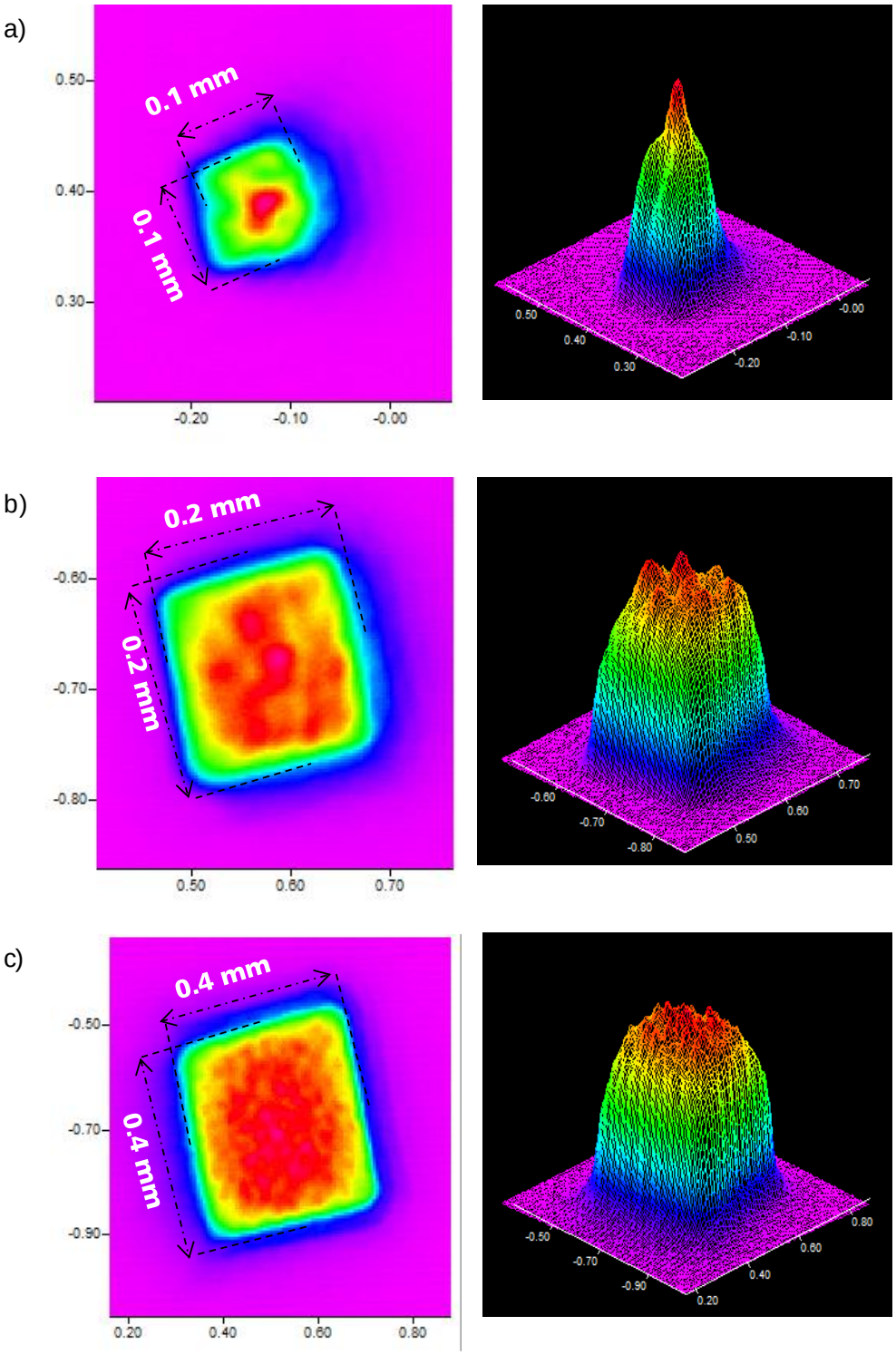

The analysis determines that zoom positions 0 mm, 16 mm and 32 mm are the ones that ensure 100x100, 200x200 and 400x400 µm² laser spot sizes, respectively. The representation of the caustics that correspond to these intensity distributions can be seen in 10.1 (Appendix).

In addition to other parameters, beam shape is also important in laser polishing [9]. Due to the orientation of the non-symmetric square core fiber, the edges of intensity distribution in the laser focus are not parallel to the machine axes, effect that needs to be compensated. The starting situation and the aiming one are shown in Figure 8 below.

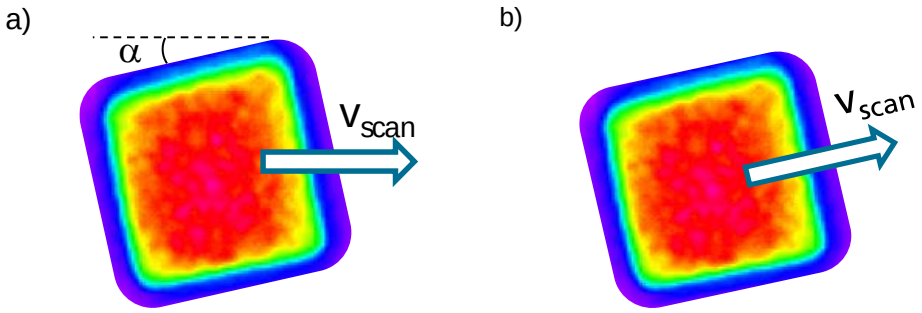

Figure 8:
Square beam advance:
a) Initial situation
b) Aimed situation

Since the intensity distribution is turned around the z-axis of the machine, the angle between the edge of the intensity distribution and the machine axis, α, needs to be measured and known. For this matter, both work piece and scan field are turned anti-clockwise in the machine. Once the tilting angle is known, the NC program is modified so that the scan velocity vector's direction is parallel to the beam's edges.

3.2.2 Laser power measurement

The laser power measurement is carried out by means of a water cooled LM-1000 power sensor by Coherent. This sensor is placed under the f-theta lens and aligned with the laser beam with the help of the PowerMax software, which provides the actual laser power output.

3.2.3 Tool definition

In this chapter all the tools employed on the three performed investigations are described attending to the type of radiation that is used: cw or pulsed.

For the macro polishing tools no attenuator is employed and tools' parameters are shown in Table 1. The Q200_TD tool is also used for executing the structuring by laser remelting investigations.

Table 1: Continuous wave operation tools parameters

Tool	Size [µm²]	Zoom Position	Z offset [mm]
Q100_TD	100x100	Zoom 0	-0.75
Q200_TD	200x200	Zoom 16	-0.5

The tools employed for micro polishing are defined through investigations carried out at a power of 500 W combined with a power attenuator. Thus, each tool definition investigation has an attenuation angle and laser power associated, so that three different stable laser spot sizes are obtained. Tools' parameters are shown in Table 2.

Table 2: Pulsed operation tool parameters

Tool	Size [µm²]	Zoom Position	Attenuation Angle [°]	Laser power [W]	Z offset [mm]
Q100_TM	100x100	Zoom 0	39.96	20	-1.75
Q200_TM	200x200	Zoom 16	39.6	60	-0.5
Q400_TM	400x400	Zoom 32	39.96	150	0

4 Methodology

4.1 Sample

4.1.1 Material

The investigated material, 1.2379, is a cold work steel commonly used in high cutting tools such as dies and punches, blanking and punching tools or cold extrusion. Furthermore, this 12% ledeburitic chromium steel combines very high wear resistance, toughness, dimensional stability and compressive strength, being suitable for a wide range of applications including cold work tooling. An overview of its chemical composition is shown in Table 3.

Table 3: Chemical composition of 1.2379+ steel [11]

Element	Cr	C	V	Mo	Fe
Mass fraction [%]	12.00	1.55	0.90	0.80	Balance

The particularity of 1.2379+ as opposed to standard 1.2379 (X153CrMoV12, AISI D2) steel is the powder metallurgical manufacturing. The advantages over the conventionally cast material includes a segregation-free and homogeneous microstructure. Those properties make it stand out as far as machine-ability, polish-ability and grind-ability are concerned. [11]

4.1.2 Preparation

For this investigation, laser polishing (cw and pulsed radiation) as well as structuring by laser remelting investigations are systematically performed on 50x75x14.5 mm³ 1.2379+ cold work steel slabs. The initial surface topography for each side of the sample is prepared mechanically by grinding, resulting in an average surface roughness of $Ra < 0.4\ \mu m$.

The experiments are carried out on flat surfaces with the previously described tools and for each tool the laser spot size, track offset dy, and residual oxygen c_{O_2} in the chamber are kept constant. Regarding laser polishing, a portion of the surface remains unaltered in order to characterize the initial surface properly.

4.1.3 Initial Surface

An example of the initial surface used for all the investigations is shown in Figure 9, where two different kind of scratches are detected.

Figure 9: Microscope picture of the initial surface

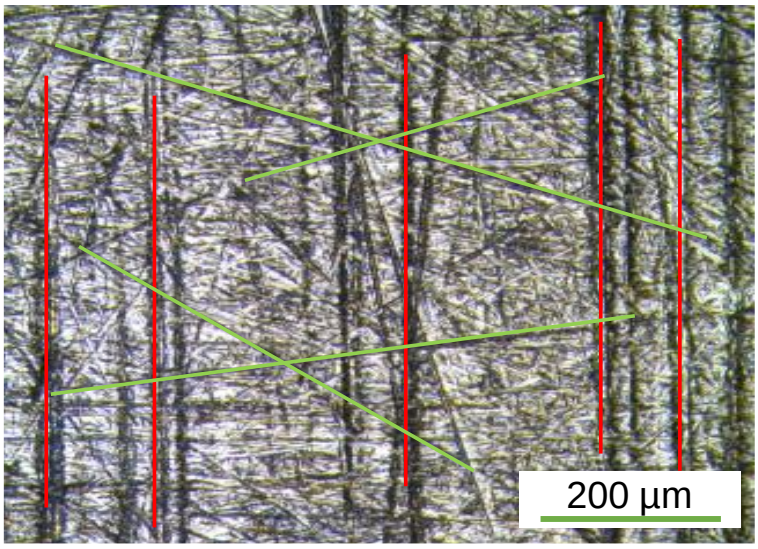

The two types of marks correspond to grinding marks and zig-zag scratches, and have been colored in red and green, respectively. These grooves are originated by the preparation process of the samples.

4.2 Surface Measurement

4.2.1 Perthometer

For the tactile roughness evaluation of the surface the Mahr M2 perthometer by Mahr is used. This instrument serves for determining two-dimensional roughness parameters by moving a diamond head stylus horizontally over the area to study. Thus, the vertical movement of the stylus determines the topography of the surface. The Ra parameter is measured in accordance with DIN EN ISO 4287, defined in **¡Error! No se encuentra el origen de la referencia.**, for determining the tactile roughness

4.1

$$Ra = \frac{1}{lr}\int_{0}^{lr} |Z(x)|\, dx$$

Figure 10:
Schematic of Ra representation

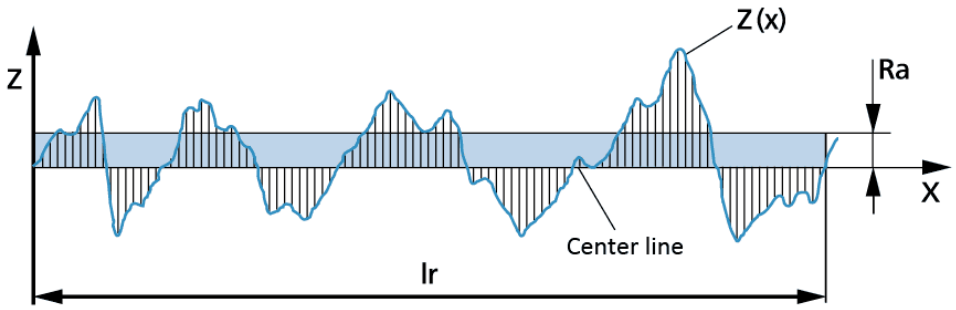

This instrument is used for measuring each specimen's initial and final tactile roughness when macro polishing. For this purpose, each field is measured twice diagonally and once perpendicularly to the polishing marks, with a cut-off of lc = 0.8 mm and a traversing length of Lt = 5.6 mm.

4.2.2 Stereo Microscope

For the optical evaluation of the surface the stereo microscope Leica M205 C by Leica Microsystems is employed. There are two objectives available: 1.0x PlanApo and 2.0x PlanApo, being the latter the one that is used. The 2.0x PlanApo objective has a maximum aperture of 0.35 and can attain an optical resolution of 1050 LP/mm (line pairs per millimeter) or 0.952 µm [12]. The latter is the one which is used for the analysis of the samples.

This stereomicroscope is also equipped with a digital camera and connected to a computer so that pictures can be easily taken with the provided Leica Application Suite software. This program allows the setting of different parameters such as light level, exposure time or intensity and shows both the magnification setting and the position of the iris diaphragm in real time, resulting in a high quality photograph.

4.2.3 White Light Interferometer

Mechanical measurement contact-based methods are often employed for quantifying the roughness of a surface. However, polishing and structuring by remelting introduce changes in roughness that cannot be sufficiently represented by those conventional mechanical methods. A spectral analysis of the surface roughness is necessary. Thus, for the 3D evaluation of surface topography the Zygo Newview 7300 Optical Surface Profiler by Zygo is used. Zygo Newview 7300 is a white light interferometer system offering fast, contactless, high-precision 3D optical profiling of surface features. As for magnification settings, 1x, 5x, 20x and

50x objectives are available in combination with 0.5x, 1x and 2x discrete zoom lenses. The vertical resolution is 3 nm, whereas the spatial one depends on the objective and ranges from 0.36 to 9.50 µm [13] . Magnification and zoom parameters among others are set by means of the provided analysis software, Zygo MetroPro.

4.3 Surface analysis

4.3.1 Roughness spectrum

When polishing, each specimen's initial and final surfaces are measured in order to characterize the experienced alterations. Using a Mahr M2 mobile perthometer the roughness Ra is determined. Additionally, the surfaces are measured with a Zygo NewView 7300 white light interferometer (WLI) with different magnifications, thus, allowing a spectral roughness analysis of the topography.

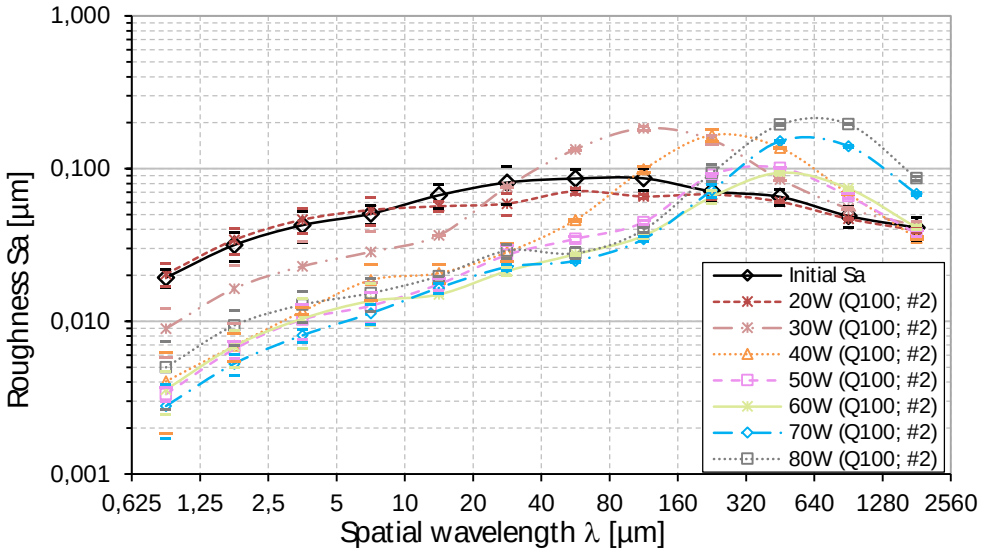

Figure 11: Sa-spectrum in dependence on laser power

Constant process parameters:
Tool: Q100_TD
dy = 20 µm
v_{scan} = 200 mm/s
n = 2 passes

A representative roughness spectrum is shown in Figure 12, where Sa roughness in function of the spatial wavelength of the surface is presented. This representation is based on Fourier transform and is used to separate waviness and form from surface roughness.

4.3.2 Structure height

When structuring by remelting, the most important parameter for characterization is structure height, h. After structuring, the topography of the structured single tracks is obtained by means of WLI (Figure 13 top).

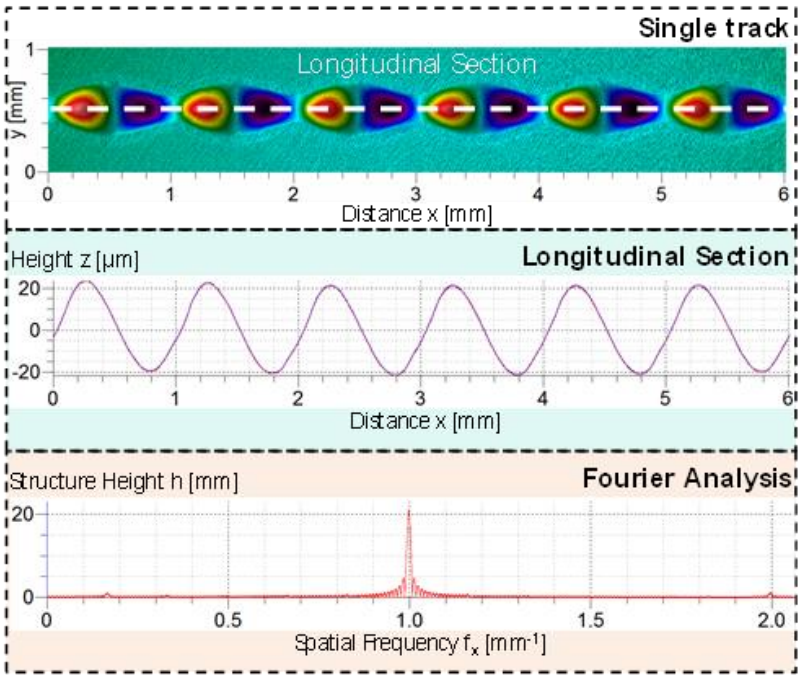

Figure 14: Schematic for single tracks analysis

Based on these measurements, structure height and wavelength of a single track are analyzed along a longitudinal section in the middle of the track (Figure 15 middle). An adapted, one-dimensional Fast Fourier Transform is used to analyze this longitudinal section in terms of spatial frequencies, phases and corresponding amplitudes (Figure 16 bottom). To precisely determine the main spatial frequency and corresponding modulation amplitude, zero-padding is used, which leads to a declining ringing effect near the dominant peaks. The spatial wavelength is the inverse of spatial frequency ($\lambda = f^{-1}$), while the amplitude equals structure height, h. For each set of experiments, six single tracks are remelted in order to increase the confidence level.

Additionally, the stereo microscope is also employed in both polishing and structuring by remelting for taking pictures of the surfaces and topographies.

5 Results of the experimental investigations

5.1 Macro laser polishing

Macro polishing involves cw operation and is performed with the TruDisk 1000. There are two kinds of investigations and two subsequent tools employed depending on the required laser spot size: 100x100 and 200x200 µm². In Table 4 a summary of the investigated laser parameters is shown.

Table 5: Summary of investigated cw macro polishing parameters

Macro polishing investigated parameters		
Laser spot size $d_{L,E}$	100 µm	200 µm
Laser power P_L	20 - 80 W	40 - 160 W
Scan velocity v_{scan}	50; 100; 200 mm/s	
Track offset dy	20 µm	40 µm
Number of passes n	1; 2; 4 passes	
Shielding gas	Argon	
Residual oxygen c_{O_2}	1000 ppm	

The selected track offsets dy correspond to a track overlap of 80% laser spot width and the minimum laser power is defined by the lack of remelting, whereas the plasma or evaporation of material is used for determining the maximum laser power. In this case, the upper P_L for the 100x100 µm² tool is limited to 80 W due to restrictions related to the machine's configuration.

Macro polishing investigations are analyzed attending to the employed number of passes (1, 2, 4 passes) and scan velocities (50, 100, 200 mm/s). Then, both Ra and Sa spectrum graphs together with microscope and WLI pictures are shown in order to describe the results.

5.1.1 Tool Q100_TD

The tool Q100_TD utilizes the laser beam source TruDisk 1000 and a quadratic fiber so that in combination with an adapted magnification of the zoom a quadratic laser beam focus of 100x100 µm² is realized. The change of surface roughness Ra parameter as laser power is increased is shown in Figure 17 for v_{scan} = 200 mm/s and laser power from 20 W up to 80 W stepwise in steps of 10 W.

Figure 17: Roughness Ra in dependence on laser power for different number of passes

Constant process parameters:
Tool: Q100_TD
dy = 20 µm
v_{scan} = 200 mm/s

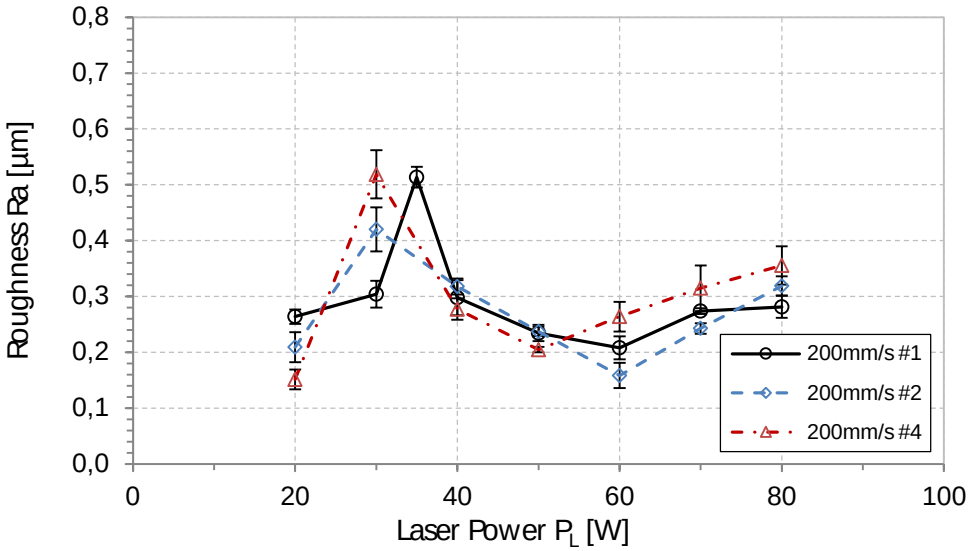

As laser power is increased, the initial roughness remains firstly unaffected for a laser power of 20 W, and then a peak followed by a local minimum is reached, after which Ra rises again. For this tool and scan velocity, the local minimums for the different investigated numbers of passes are around 50 - 60 W, achieving the biggest reduction of roughness to Ra = 0.16 ± 0.02 µm with n = 2 passes and P_L = 60 W.

With regard to the results achieved for n = 2 passes, a comparison among all roughness obtained with the three investigated scan velocities is shown in Figure 18. Then, it is determined that the combination of v_{scan} = 200 mm/s and n = 2 passes gives rise to the smallest roughness Ra, which is described in further detail below.

Figure 18: Roughness Ra in dependence on laser power for different scan velocities

Constant process parameters:
Tool: Q100_TD
dy = 20 µm
n = 2 passes

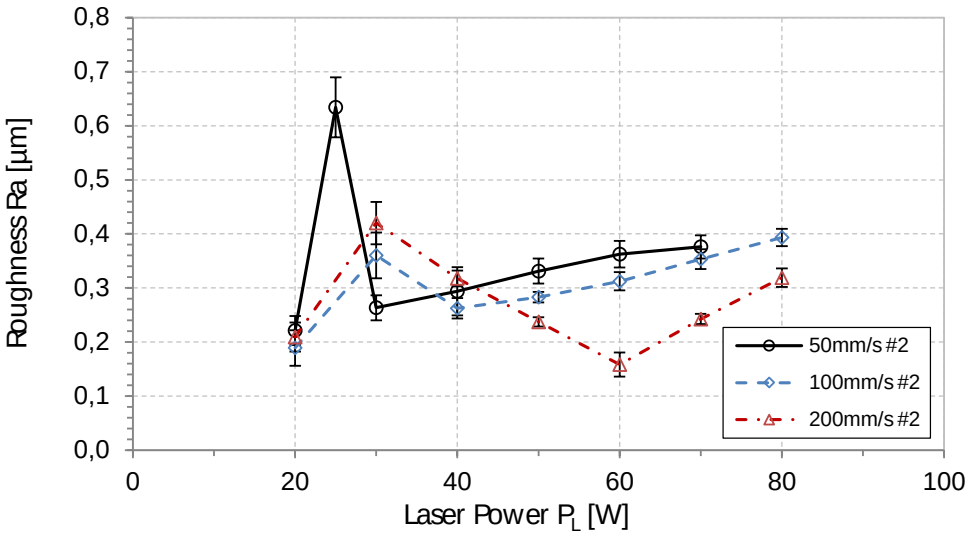

The Sa spectrum related to processing with v_{scan} = 200 mm/s and n = 2 passes is shown in Figure 19, showing a main trend as P_L is increased, in which initial Sa is decreased for λ < 160 µm up to 70 W, while it rises for bigger wavelengths.

Figure 19:
Sa-spectrum in dependence on laser power

Constant process parameters:
Tool: Q100_TD
dy = 20 µm
v_{scan} = 200 mm/s
n = 2 passes

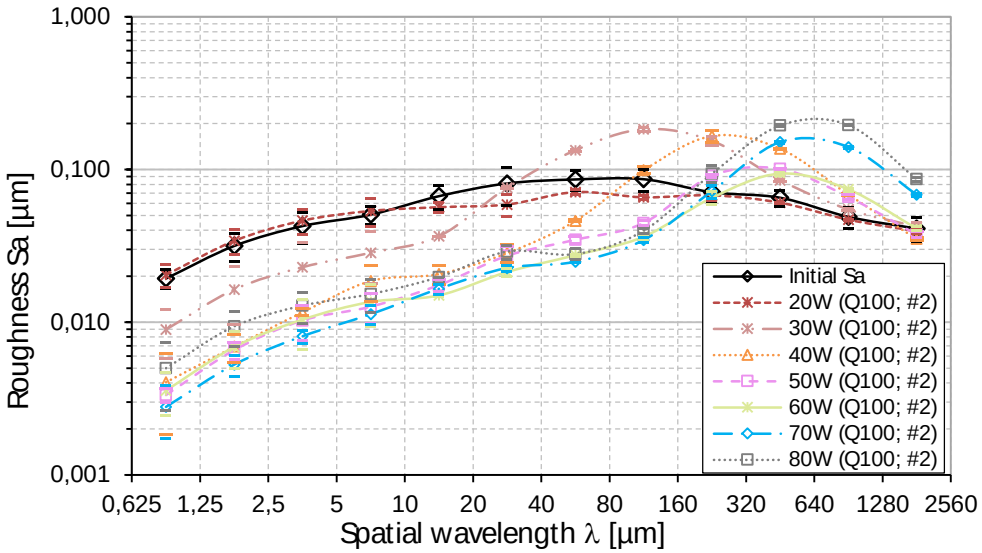

In addition, for laser powers ranging from 30 - 50 W it shows how gradually bigger wavelength ranges are affected. This effect is visible in the microscope pictures in Figure 20 that match with the mentioned range of powers, going from a surface with a high number of defects (P_L = 30 W) to a homogeneous one (P_L = 50 W). Along this phase and regarding laser powers from 30 - 40 W, there is a higher meso roughness due to the appearance of defects and irregularities (see Figure 21). Another aspect to highlight is the presence of traces of oxide, which correspond to the darker areas in the microscope pictures regarding 80 W.

Figure 20:
Microscope pictures of surfaces after laser polishing with different laser powers

Constant process parameters:
Tool: Q100_TD
dy = 20 µm
v_{scan} = 200 mm/s
n = 2 passes

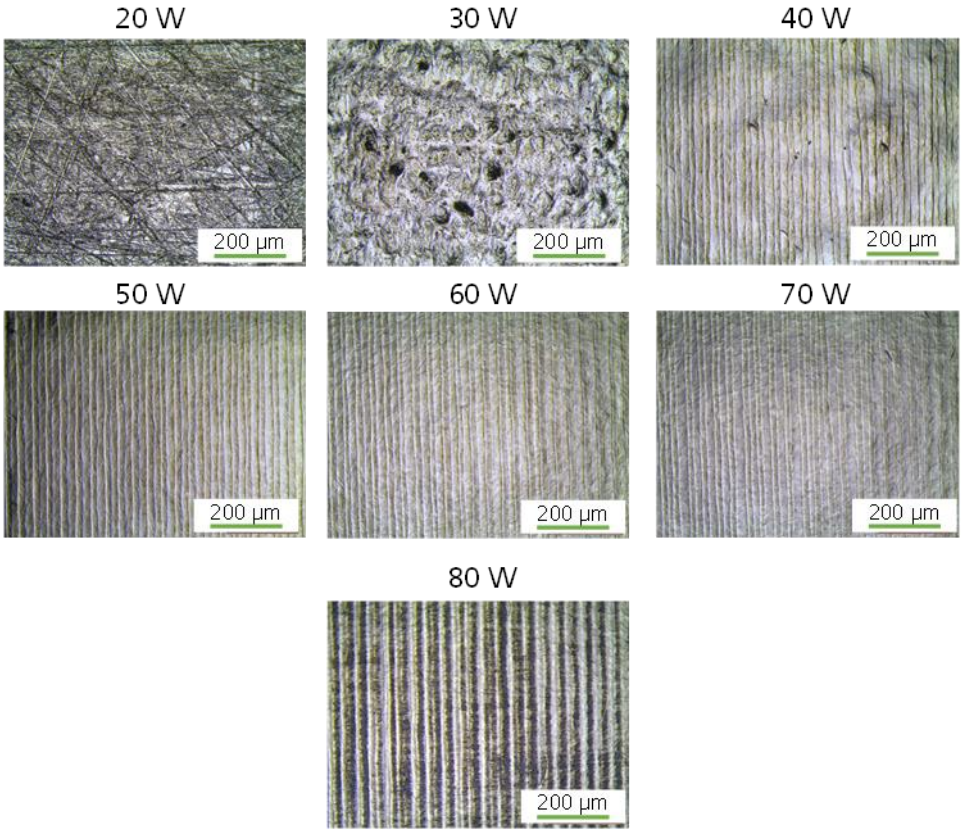

Figure 21:
Sa-spectrum in dependence on laser power

Constant process parameters:
Tool: Q100_TD
dy = 20 µm
v_{scan} = 200 mm/s
n = 2 passes

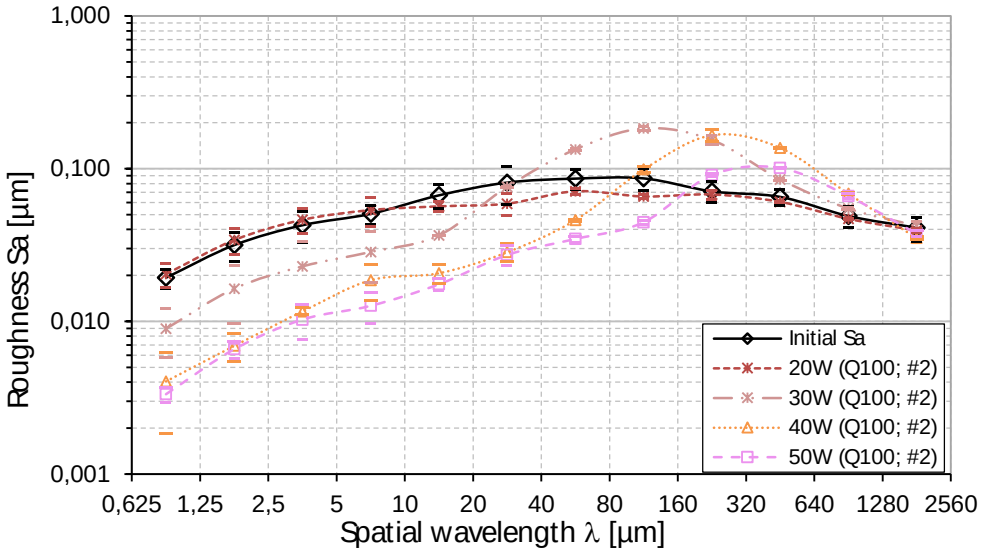

As for the smallest attained local Sa, laser powers from 50 - 70 W give the smallest results for wavelengths up to 160 µm. A graphic comparison between the initial

surface and the field investigated with 70 W, which is representative of the smallest obtained roughness spectrum, is presented in Figure 22.

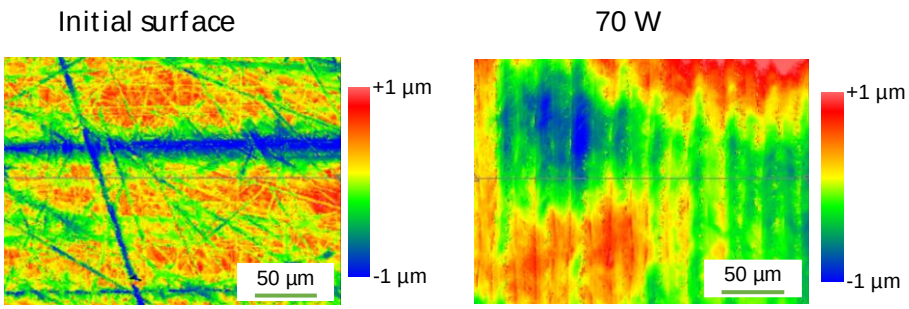

Figure 22: WLI pictures for initial surface and 70 W

Constant process parameters:
Tool: Q100_TD
dy = 20 µm
v_{scan} = 200 mm/s
n = 2 passes

The other investigated numbers of passes for v_{scan} = 200 mm/s present similar results, but P_L = 80 W also gives a small surface roughness Sa (see Figure 58 (10.2 - Appendix)). Then, the roughness is decreased for this scan velocity and spatial wavelengths below 20 µm when processing with n = 1 pass; 50 - 60 W or n = 2 passes; 70 W, whereas the combination n = 4 passes; 70 - 80 W gives the smallest results within the range 20 < λ < 160 µm.

Processing with scan velocities of 50 and 100 mm/s gives similar results to 200 mm/s but there are some particularities that are therefore explained:

On the one hand and regarding the results using 50 mm/s, when analyzing Ra as function of P_L, the local minima are obtained for 30 - 40 W. Among those minima, the smallest roughness is achieved for n = 1 pass results at 40 W, Ra = 0.25 ± 0.01 µm, but it is close to the lowest roughness obtained with n = 2, Ra = 0.26 ± 0.02 µm at 30 W. Moreover and concerning the roughness spectrum, the usage of a laser power of 40 and 50 W leads to the smallest roughness results for n = 1, while 30 W is added to those two laser powers when processing with 2 and 4 passes. Comparing the three sets of parameters, using n = 2 passes reduces Sa below λ = 2.5 µm. The roughness spectrum for wavelength ranges of 2.5 - 40 µm and 40 - 160 µm is decreased at 50 W with n = 1 and 4 passes, respectively (see Figure 56 (10.2 - Appendix)).

On the other hand and with regard to processing with 100 mm/s, a local minimum is achieved for the three combinations of passes and 40 W, obtaining Ra = 0.24 ± 0.03 µm for n = 1 pass and differing very little from roughness achieved with n = 2 (Ra = 0.26 ± 0.02 µm) and 4 passes (Ra = 0.25 ± 0.02 µm). The set of parameters that achieves the smallest roughness spectrum Sa for λ < 10 µm is 60 W; n = 2 passes, attaining also the lowest roughness Sa for 10 < λ < 160 µm but presenting similar results to processing with n = 4; 50 W. (see Figure 57 (10.2 - Appendix))

Furthermore, initial roughness is decreased for wavelengths up to 80 µm, 50 and 100 mm/s scan velocities and n = 1 pass. However, for the other investigated numbers of passes, the wavelength range that is affected increases up to 160 µm. That does not apply to a scanning velocity of v_{scan} = 200 mm/s.

5.1.2 Tool Q200_TD

The tool Q200_TD utilizes the laser beam source TruDisk 1000 and a quadratic fiber so that in combination with an adapted magnification of the zoom a quadratic laser beam focus of 200x200 µm² is realized. Regarding the 200x200 µm² laser spot size tool (Q200_TD tool), the dependency of Ra on laser power is qualitatively the same as described for the previous tool. By comparing the different scan velocities, it is observed that v_{scan} = 200 mm/s gives rise to smaller roughness, as it is shown in Figure 23 - a. Moreover, the smallest roughness attained with that scan velocity, Ra = 0.17 ± 0.01 µm, corresponds to P_L = 120 W; n = 2 passes, as it is appreciated in Figure 23 - b. Thus, v_{scan} = 200 mm/s; n = 2 passes is the set of parameters employed for describing the performance of the present tool.

Figure 23:
Roughness Ra in dependence on laser power for different:
a) scan velocities
b) number of passes

Constant process parameters:
Tool: Q200_TD
dy = 40 µm
a) n = 2 passes
b) v_{scan} = 200 mm/s

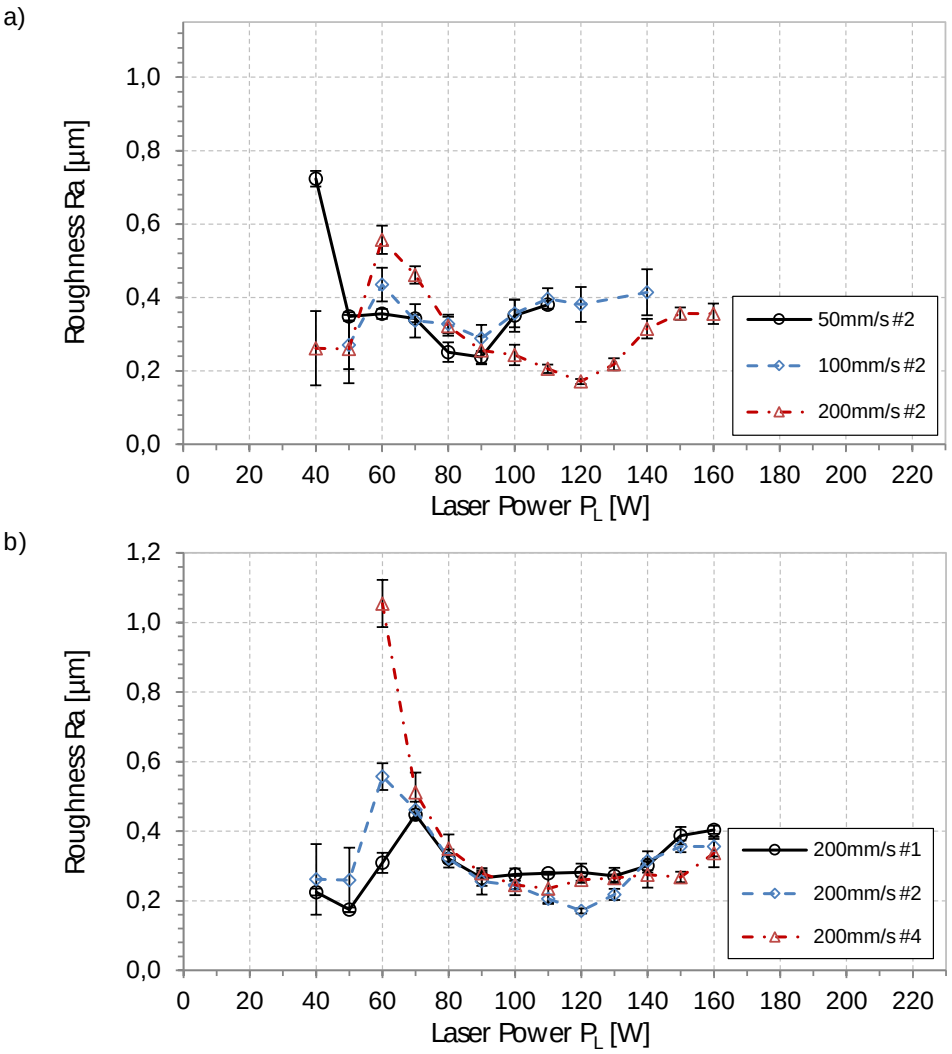

In an analogue way to the tool Q100_TD, the Sa spectrum shown in Figure 24 presents the same dependency on P_L, Sa below λ = 160 µm is lowered up to 150 W while continuously increased above the mentioned wavelength. When P_L = 160 W is reached, micro roughness increases. Besides, there is also a range of powers, from 60 - 90 W, with a higher meso roughness and gradually bigger wavelengths affected.

Figure 24:
Sa-spectrum in dependence on laser power

Constant process parameters:
Tool: Q200_TD
dy = 40 µm
v_{scan} = 200 mm/s
n = 2 passes

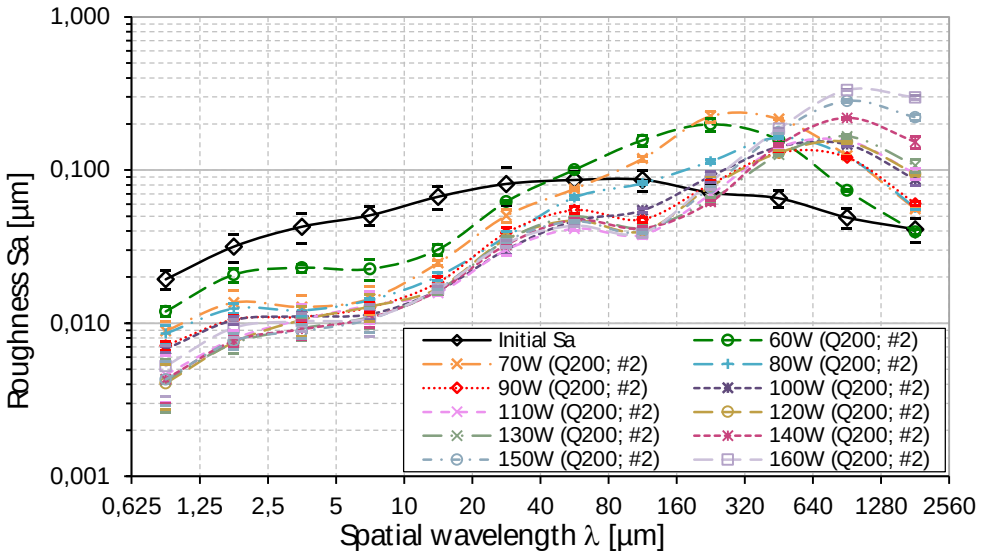

In this case, with laser powers ranging from 110 - 150 W the smallest micro roughness with $\lambda < 5$ µm is achieved, whereas for $5 < \lambda < 160$ µm the range widens up to 90 - 160 W. An example of the obtained surface is shown in Figure 25 below:

Figure 25:
WLI pictures for initial surface and 140 W

Constant process parameters:
Tool: Q200_TD
dy = 40 µm
v_{scan} = 200 mm/s
n = 2 passes

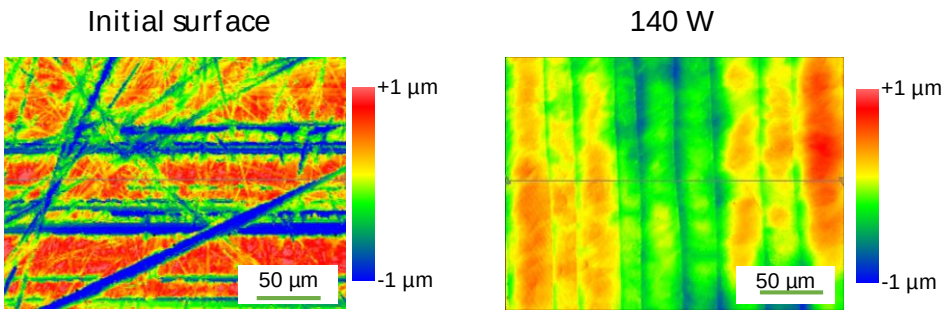

The results after processing the sample with one and four passes show the same general tendency for Sa when laser power is increased. However, using n = 1 pass does not attain lower Sa than the initial for wavelengths above 80 µm, while processing with n = 2 and 4 passes goes up to 160 µm. Besides, the laser power range that gives smaller roughness for n = 1 pass and $\lambda < 80$ µm is $80 < P_L < 140$ W. Alternatively, processing with n = 4 passes makes Sa substantially bigger for $\lambda < 5$ µm compared to n = 1 and 2 passes' results as far as micro roughness is concerned. (See Figure 62)

Figure 26:
Sa-spectrum in dependence on laser power

Constant process parameters:
Tool: Q200_TD
dy = 40 µm
v_{scan} = 200 mm/s
a) n = 1 pass
b) n = 4 passes

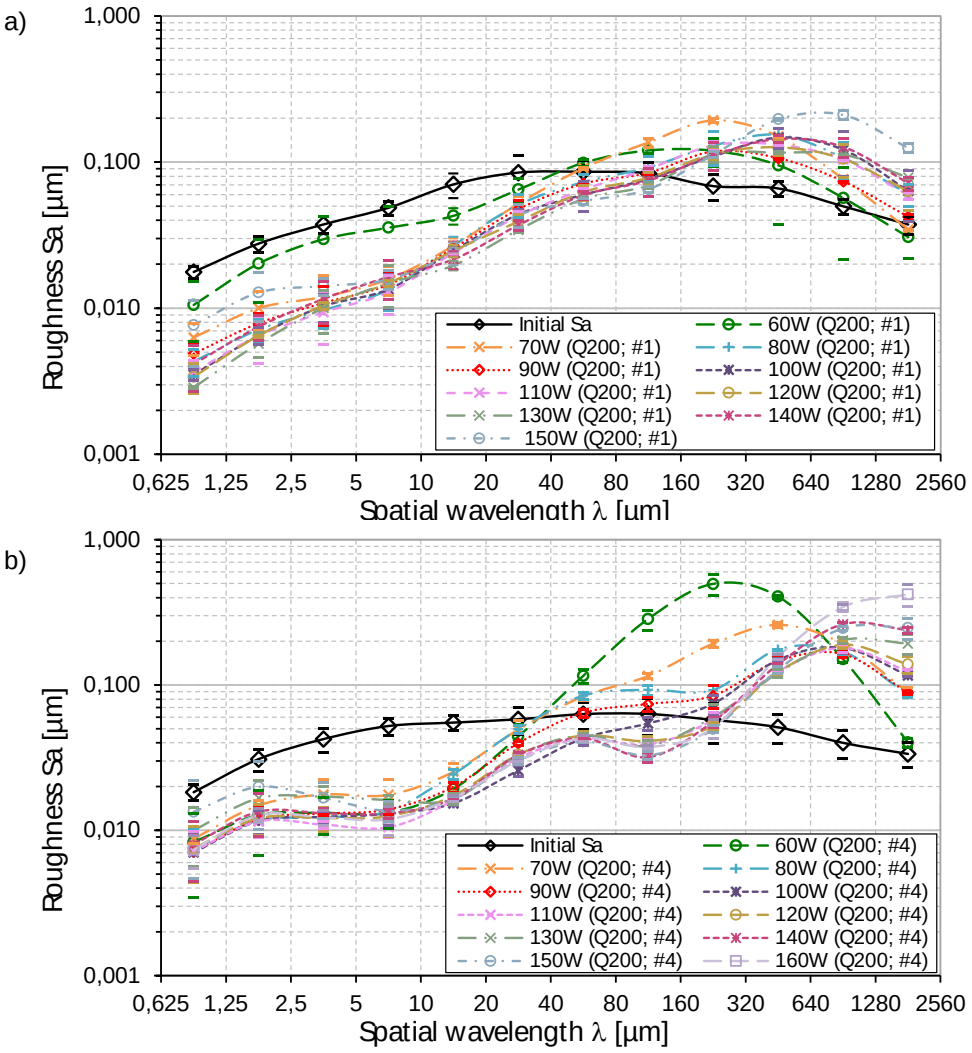

With regard to the other investigated scan velocities, they show the same qualitative results in dependence on laser power. In both cases, the local minimum Ra is obtained with four passes: Ra = 0.21 ± 0.04 µm and Ra = 0.26 ± 0.02 µm for 50 mm/s; 80 W and 100 mm/s; 90 W, respectively. However, this roughness is close to those that correspond to one or two passes. Thus, with 50 mm/s a roughness Ra = 0.24 ± 0.02 µm (n = 2 passes; 90 W) is also achieved, whereas with 100 mm/s Ra = 0.29 ± 0.05 µm (n = 1 pass; 90 W) and Ra = 0.29 ± 0.04 µm (n = 2 passes; 90 W) are obtained. Identically to what is observed at v_{scan} = 200 mm/s, using n = 1 pass lowers initial roughness up to 80 µm, while processing with n = 2 and 4 passes also affects the range of 80 < λ < 160 µm. (See Figure 59)

Figure 27:
Roughness Ra in dependence on laser power for different number of passes

Constant process parameters:
Tool: Q200_TD
dy = 40 µm
a) v_{scan} = 50 mm/s
b) v_{scan} = 100 mm/s

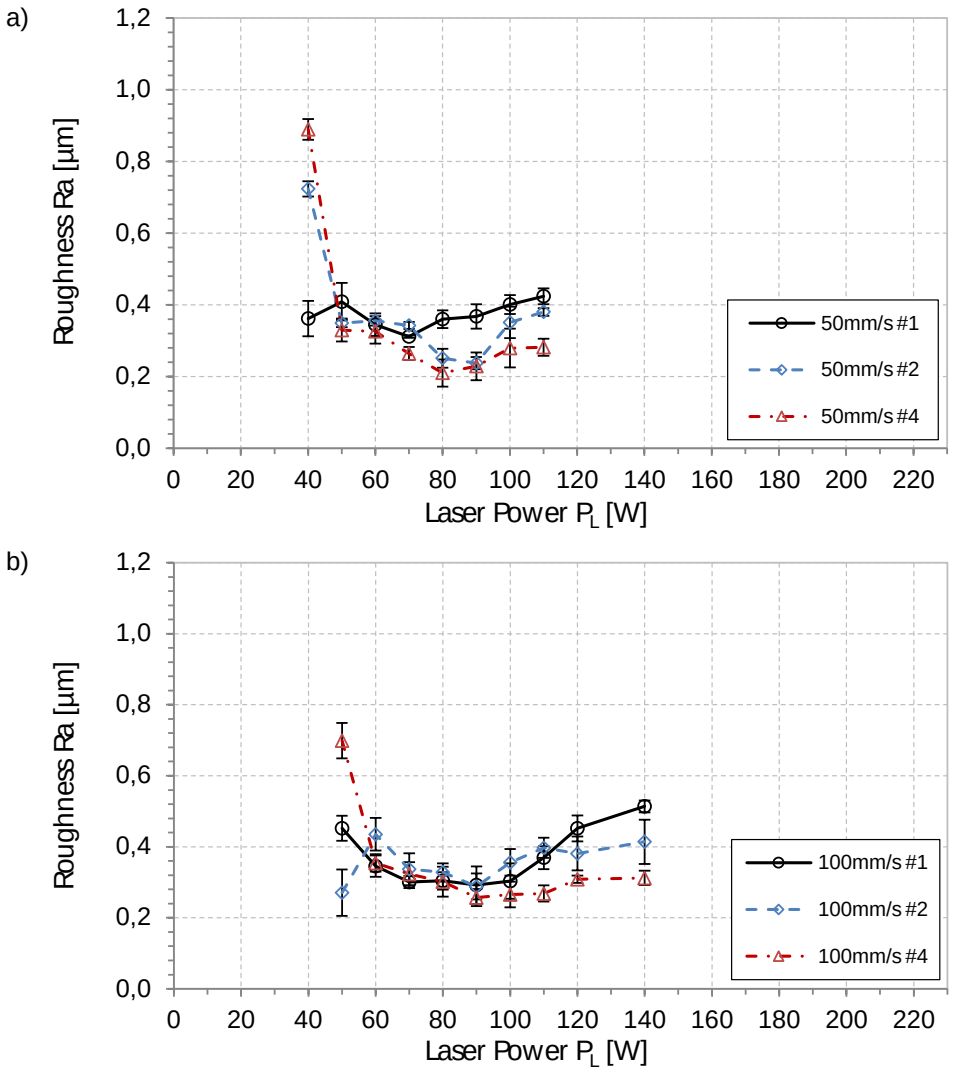

Concerning 50 mm/s, laser power from 70 - 90 W give a smaller micro roughness for one pass, whereas the range for two passes widens up to 60 - 110 W and is reduced to 60 W when processing with four passes. Among all, processing using n = 1 pass especially lowers Sa for wavelengths below 10 µm, while using n = 2; 70 W makes Sa smaller for $10 < \lambda < 160$ µm. However, laser polishing using 50 mm/s barely affects initial Sa below 5 µm compared to the results of the other scan velocities. (See Figure 28)

Figure 28:
Sa-spectrum in dependence on laser power

Constant process parameters:
Tool: Q200_TD
dy = 40 µm
v_{scan} = 50 mm/s
a) n = 1 pass
b) n = 2 passes
c) n = 4 passes

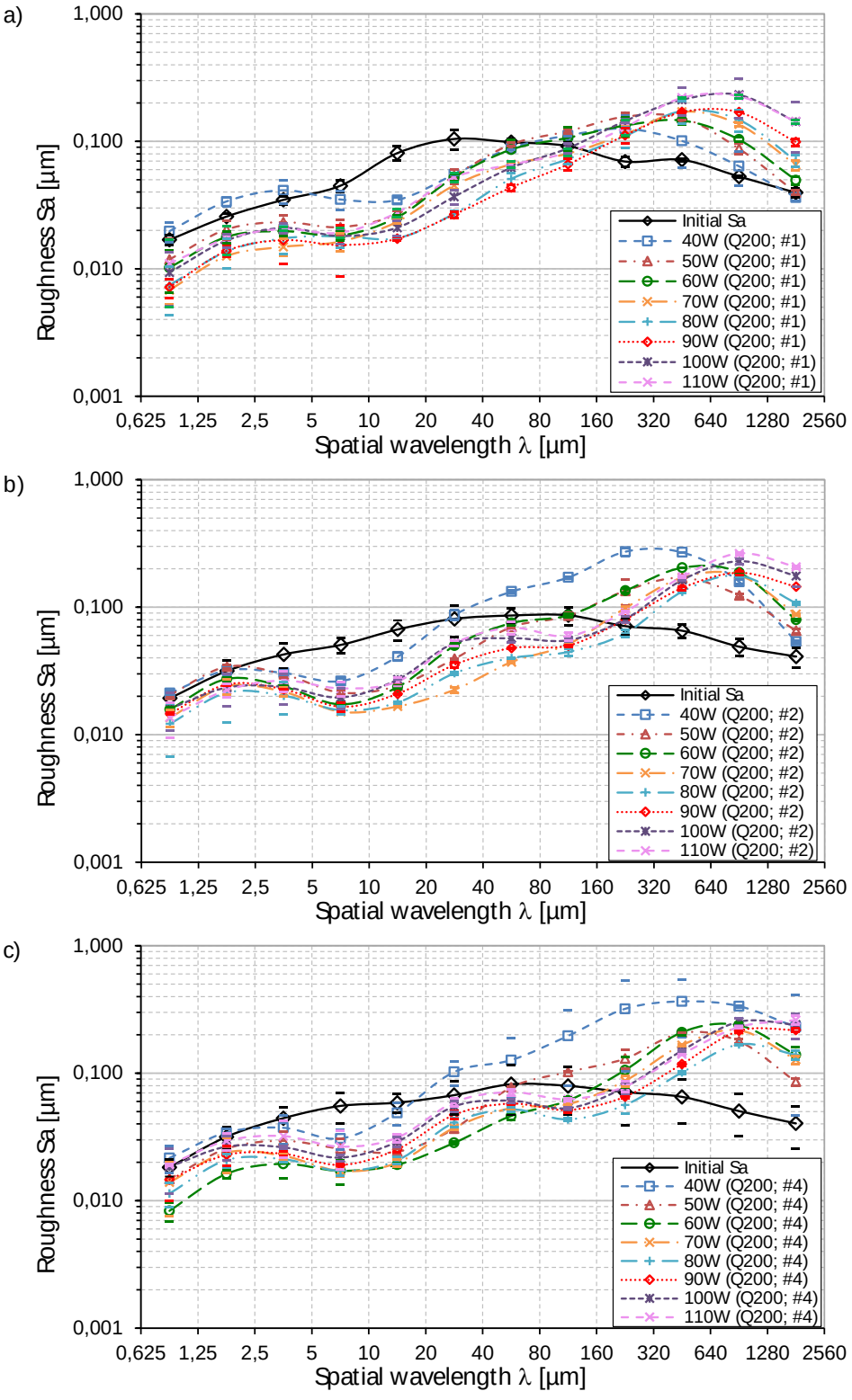

As for the 100 mm/s scan velocity, processing with laser powers from 90 - 140 W makes Sa smaller for 10 < λ < 80 µm (n = 1 pass) and it goes up to 160 µm using n = 2 passes; 110 - 160 W. The roughness spectrum regarding wavelengths below 5 µm is lowered with 90 < P_L < 110 W and one pass, while the combination of n = 2 passes and 100 - 140 W attains smaller roughness results for wavelengths between 5 and 40 µm. As for the 40 - 160 µm wavelength range, n = 2 passes; 90 - 160 W, as well as n = 4 passes; 100 - 160 W present similar results. (See Figure 29)

Figure 29:
Sa-spectrum in dependence on laser power

Constant process parameters:
Tool: Q200_TD
dy = 40 µm
v_{scan} = 100 mm/s
a) n = 1 pass
b) n = 2 passes
c) n = 4 passes

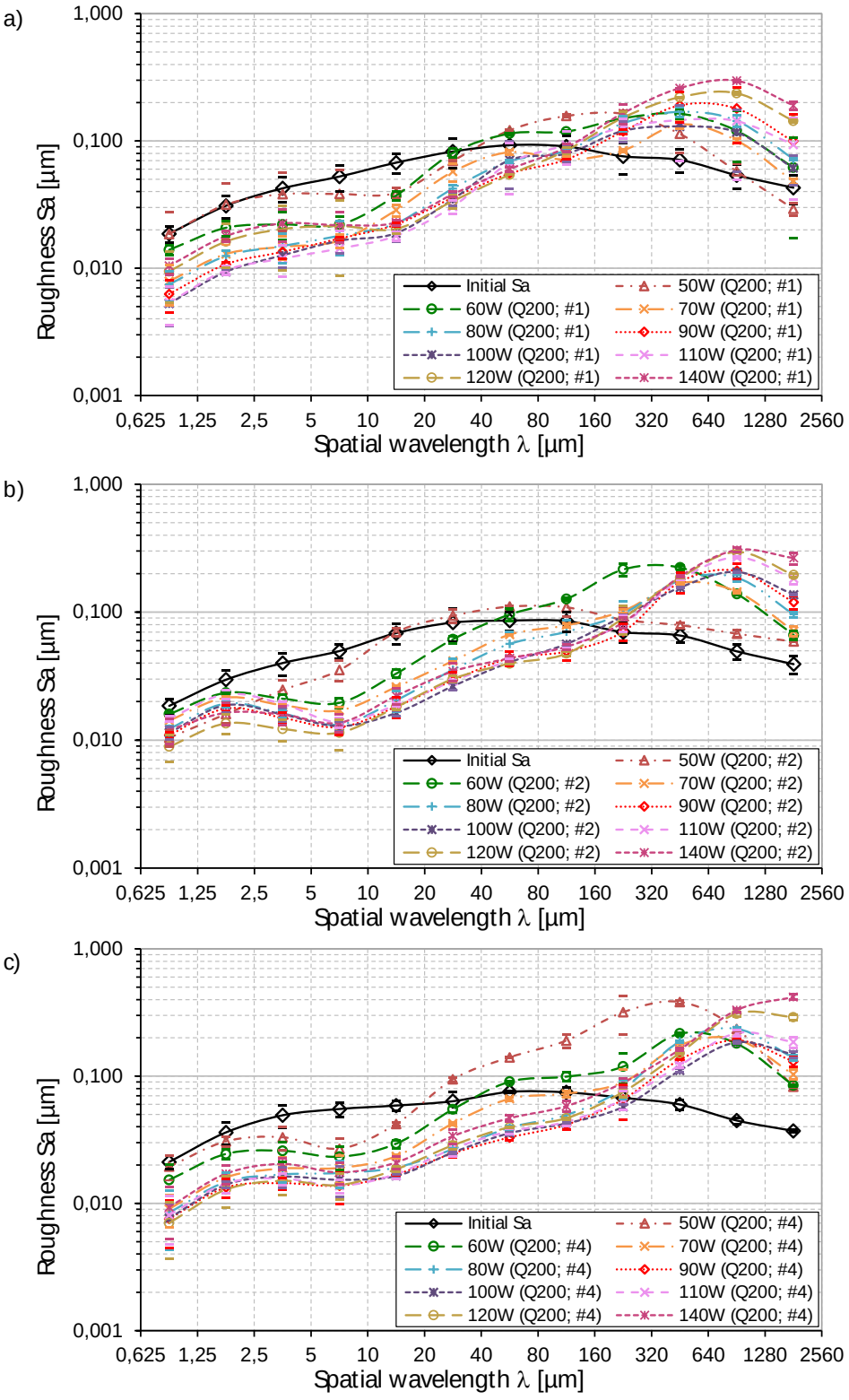

The present comparison is carried out with the support of Figure 30, where the combinations of process parameters that lead to the smallest spectral roughness have been selected. Hence, processing with laser powers from 40 - 80 W and from 70 - 160 W gives the lowest roughness results for Q100_TD and Q200_TD tools, respectively. The graphs only include the wavelength range whose roughness spectrum is lowered ($\lambda < 160$ µm).

As far as the Q100_TD tool is concerned and always referring to the laser powers that give a smaller roughness, smaller Sa is attained for spatial wavelengths below 160 µm when increasing the scan velocity. The results obtained for wavelengths below 20 µm are considerably consistent, with a similar resulting surface roughness for one and two passes, especially for v_{scan} = 100 and 200 mm/s. However, for v_{scan} = 50 mm/s a slight deviation within a wavelength range of 5 - 40 µm is observed, where the smallest roughness is achieved locally for n = 1 pass. As for $40 < \lambda < 160$ µm, resulting surface roughness for two and four passes is smaller than for one pass. However, n = 4 does not result in a considerably smaller meso roughness when compared with n = 2, being virtually identical for v_{scan} = 100 and 200 mm/s. Hence, compared to two passes, polishing with four passes does not achieve a smaller roughness spectrum. Thus, the smallest local roughness for wavelengths below λ=40 µm is obtained with v_{scan} = 200 mm/s; n = 1 or 2 passes; $50 < P_L < 70$ W. In addition, n = 2 also gives the minimum local Sa at $40 < \lambda < 160$ µm but with laser powers ranging from 60 - 80 W.

With regard to the Q200_TD tool and considering again the laser powers that give the smallest Sa results, increasing the scan velocity decreases the smallest local Sa up to λ = 20 µm. Besides, one pass attains the smallest roughness results for $\lambda < 5$ µm. For wavelengths from 5 - 160 µm, processing with n = 2 and 4 passes conforms a consistent group of roughness results and achieves the biggest local reduction. Hence, micro roughness for $\lambda < 5$ µm is minimum when n = 1 pass and v_{scan} = 200 mm/s, while $5 < \lambda < 160$ µm Sa is minimized with n = 2 and 4 passes for scan velocities of 100 and 200 mm/s.

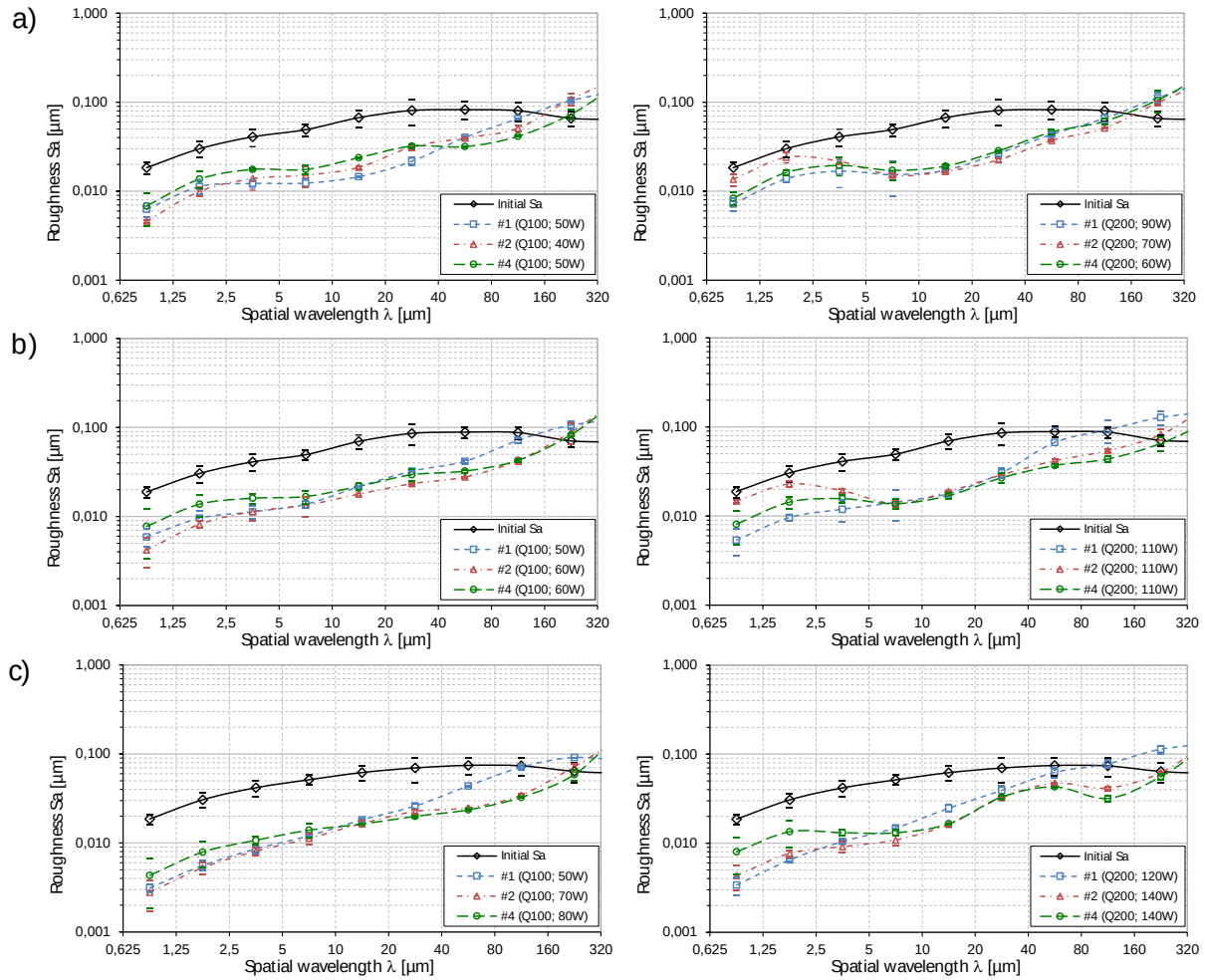

Figure 31: Representative Sa spectrum in dependence on laser power and number of passes for: a) v_{scan} = 50 mm/s ; b) v_{scan} = 100 mm/s; c) v_{scan} = 200 mm/s

5.1.3 Discussion

There are some similarities that both tools share, which are related to the trend as laser power is increased, and some correspondences that are established between the microscope pictures and the roughness spectrums. Thus, along all the experiments spectral roughness below $\lambda = 160\,\mu m$ is enhanced until there is oxidation, which affects micro roughness making it increase. This conclusion comes from the presence of oxide at high powers, leading to the hypothesis that there is a common transition phase starting with low laser powers and with a higher meso roughness, after which a homogeneous surface is achieved. Along this transition, bigger spatial wavelengths are affected as laser power is increased.

It is also concluded that processing with four passes does not give any further improvement compared to one or two passes. On the one hand, processing with two passes attains the biggest roughness improvement all along the whole spectrum from 0.625 - 160 µm for the Q100_TD tool. On the other hand and regarding the Q200_TD tool, using one pass achieves smaller micro roughness results than the other number of passes for wavelengths below 5 µm while employing two passes results in improvements within the range from 5 - 160 µm. Comparing both investigated tools' results, it is concluded that slightly smaller roughness results are attained with Q100_TD tool, v_{scan} = 200 mm/s and n = 2 passes. This coincides with the smallest Ra result, Ra = 0.16 ± 0.02 µm.

5.2 Micro laser polishing

Micro polishing implies pulsed laser radiation and is investigated with the TruMicro 7051. A summary of the used laser parameters is shown in Table 6.

Table 6: Summary of investigated micro polishing parameters

Micro polishing investigated parameters			
Laser spot size $d_{L,E}$	100 µm	200 µm	400 µm
Fluence	3 - 12 J/cm²		
Pulse frequency f_P	20 kHz		
Scan velocity v_{scan}	200 mm/s	400 mm/s	800 mm/s
Track offset dy	10 µm	20 µm	40 µm
Number of passes n	1 pass		
Shielding gas	Argon		
Residual oxygen c_{O_2}	1000 ppm		

The pulse duration t_p is 1 µs, and the track offsets dy match a track overlap of 90% laser spot width. The laser power variation is carried out by varying the fluence stepwise in steps of 1 J/cm² for the three tools within a range of 3 - 12 J/cm². The obtained results are then compared taking the fluence as a basis.

As far as the micro polishing experiments are concerned and as it has been previously mentioned, the analysis of the results is based on the fluence parameter. The corresponding laser power and energy per unit length are shown in 10.3 (Appendix).

5.2.1 Tool Q100_TM

The tool Q100_TM is utilized with the laser beam source TruMicro 7051 and a quadratic fiber so that in combination with an adapted magnification of the zoom a quadratic laser beam focus of 100x100 µm² is realized. An overview of the obtained surfaces is shown in Figure 32.

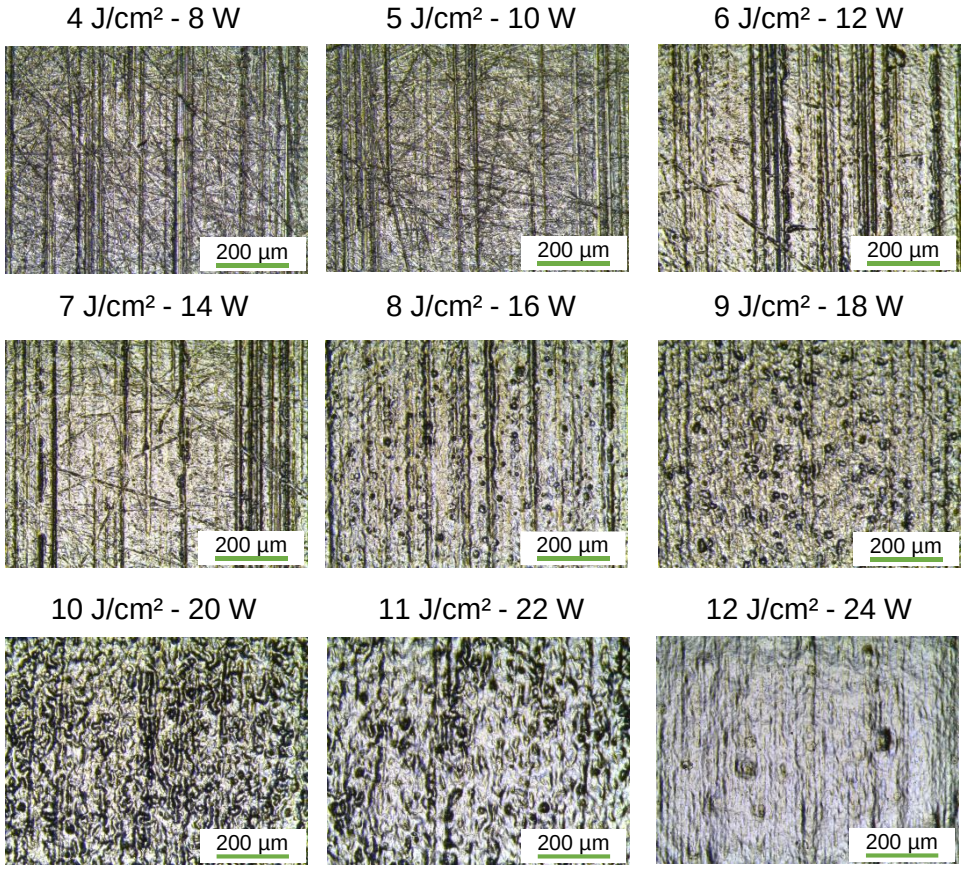

Figure 32:
Microscope pictures of surfaces after laser polishing with different fluences

Constant process parameters:
Tool: Q100_TM
dy = 20 µm
v_{scan} = 100 mm/s
n = 1 pass

In the first two images (4 and 5 J/cm²), two kinds of initial surface structures are distinguished: vertical grinding marks and zig-zag scratches. As energy per unit surface is increased, zig-zag scratches are smoothed and first defects such as holes appear when reaching 8 J/cm². Then, vertical grinding marks are also dampened as well as the number of defects increases when the fluence is 10 J/cm². Finally, the number of defects decrease while their size is increased and 12 J/cm² presents the smallest micro roughness.

Additionally, the roughness spectrum is also provided in Figure 33. It is appreciated how the surface gets affected by the process for fluences higher than 4 J/cm²,

lowering roughness with fluences above 5 J/cm², while increasing it for λ > 40 µm. In addition, the critical spatial wavelength differs for the diverse fluences, reaching λ = 40 µm with 12 J/cm². However for fluences below 12 J/cm², the roughness between wavelengths from 10 - 40 µm is close to the initial roughness within the standard deviation and only λ < 10 µm gets smoothed. Besides, there is a big difference between 11 and 12 J/cm².

Figure 33:
Sa-spectrum in dependence on fluence

Constant process parameters:
Tool: Q100_TM
dy = 10 µm
v_{scan} = 200 mm/s
n = 1 pass

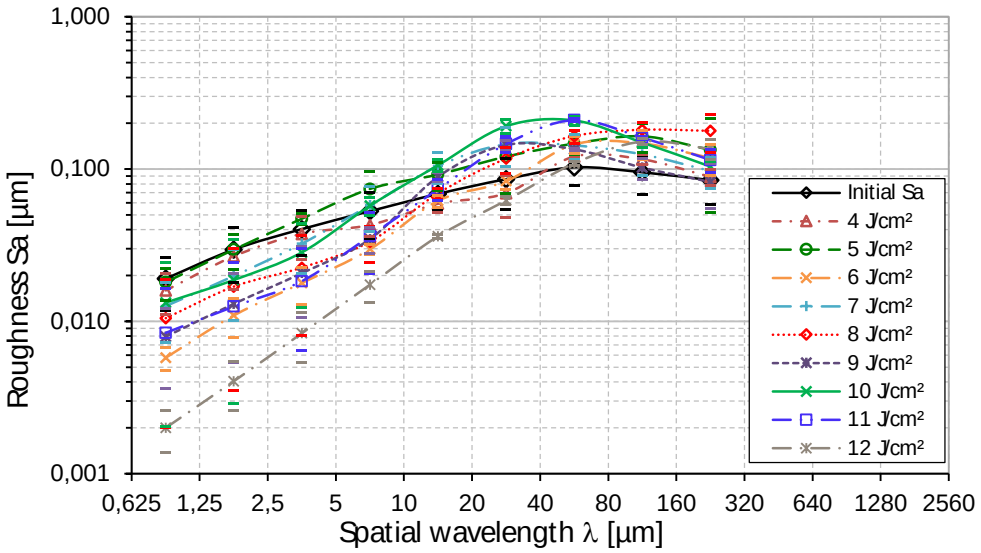

Although processing with 12 J/cm² gives the smallest Sa results, as far as fluence is increased no concrete tendency is concluded. However, all fluences have a similar form but 10 J/cm², which presents a higher roughness for spatial wavelengths between 10 and 80 µm.

The analysis with the WLI pictures show that the zig-zag scratches are smoothed and there are defects that become visible as holes (blue) and bumps (red) (see Figure 34).

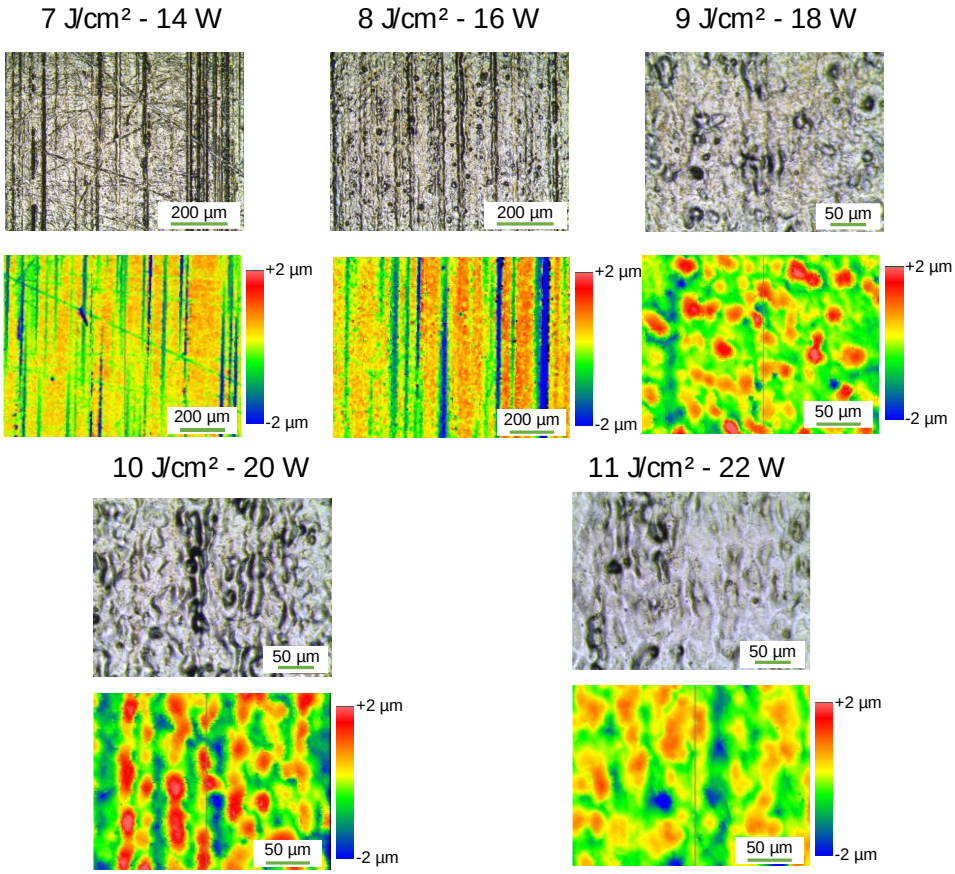

Figure 34:
Microscope (up) and WLI (down) pictures for different fluences

Constant process parameters:
Tool: Q100_TM
dy = 10 µm
v_{scan} = 200 mm/s
n = 1 pass

Finally, a comparison between the initial surface and the one regarding the lowest micro roughness achieved (12 J/cm²) is shown in Figure 35.

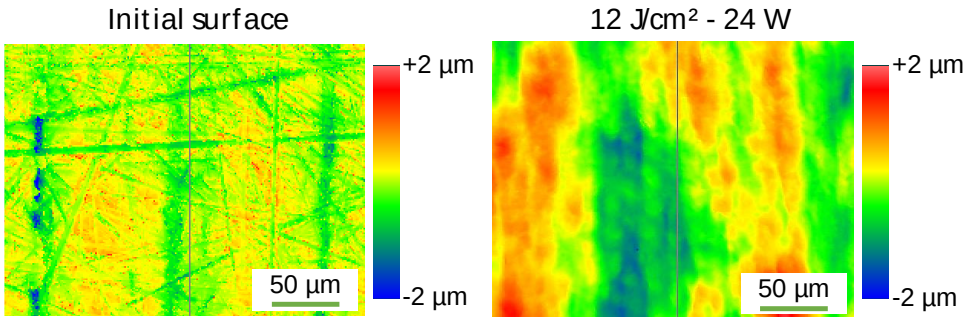

Figure 35:
WLI pictures for initial surface and 12 J/cm²

Constant process parameters:
Tool: Q100_TM
dy = 10 µm
v_{scan} = 200 mm/s
n = 1 pass

With a fluence output of 12 J/cm² the initial roughness is reduced within a spatial wavelength range up to 40 µm.

5.2.2 Tool Q200_TM

The tool Q200_TM utilizes the laser beam source TruMicro 7051 and a quadratic fiber so that in combination with an adapted magnification of the zoom a quadratic laser beam focus of 200x200 µm² is realized. The microscope pictures of the resulting surfaces are presented in Figure 36, showing a qualitatively similar dependence of resulting surface roughness on fluence as described for the Q100_TM tool. However, there is a contrast regarding the fluences that is described henceforth: zig zag scratches are smoothed when reaching 6 J/cm², and the highest number of defects is observed on the results of 7 J/cm².

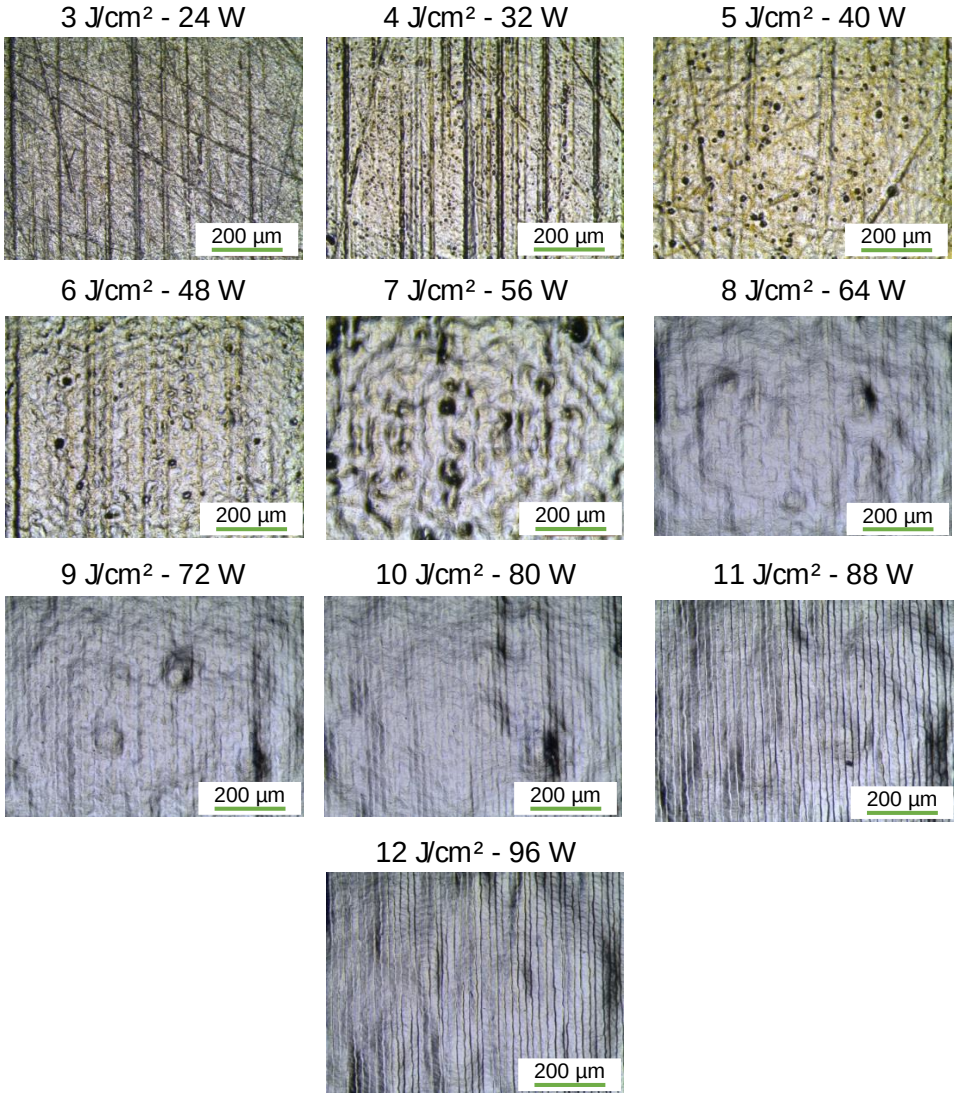

Figure 36:
Microscope pictures of surfaces after laser polishing with different fluences

Constant process parameters:
Tool: Q200_TM
dy = 20 µm
v_{scan} = 400 mm/s
n = 1 pass

In addition, the Sa spectrum of the resulting surfaces is also provided in Figure 37. On the one hand, when micro polishing, spatial wavelengths over 320 µm remain unaffected. Roughness obtained for fluences ranging from 3 to 6 J/cm² is below the initial roughness for spatial wavelengths between 40 and 320 µm. There is also an anomaly related to 7 J/cm², which presents higher roughness for 40 µm < λ < 80 µm.

On the other hand, it is detected that for fluences up to 10 J/cm², as energy per unit area is increased, smaller Sa is obtained for λ < 40 µm but higher for λ > 40 µm. For higher fluences, such as 11 and 12 J/cm², bigger micro roughness is experienced. Moreover, similarities are perceived for three different groups of fluence regimes:

- For fluences of 4, 5 and 6 J/cm² a gradual lowering of surface roughness in comparison to initial roughness is achieved for 5 µm < λ < 40 µm.
- Resulting surface roughness using fluences from 7 - 10 J/cm² is within the standard deviation for the spatial wavelength interval 0.625 µm < λ < 10 µm.
- Resulting surfaces processed with fluences of 11 and 12 J/cm² show less inhomogeneities compared to the previous groups. In addition, the results are within the standard deviation for spatial wavelengths ranging 0.625 µm < λ < 160 µm.

Figure 37:
Sa-spectrum in dependence on fluence

Constant process parameters:
Tool: Q200_TM
dy = 20 µm
v_{scan} = 400 mm/s
n = 1 pass

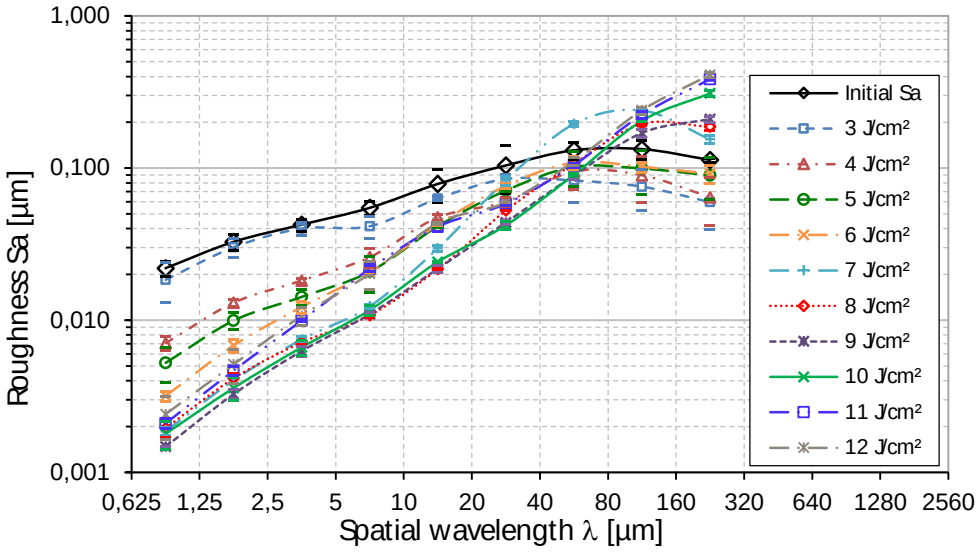

The smallest roughness corresponds to 9 and 10 J/cm², which are very similar and reduce initial roughness for $\lambda < 40$ µm. This can be detected in the microscope and WLI pictures in Figure 38.

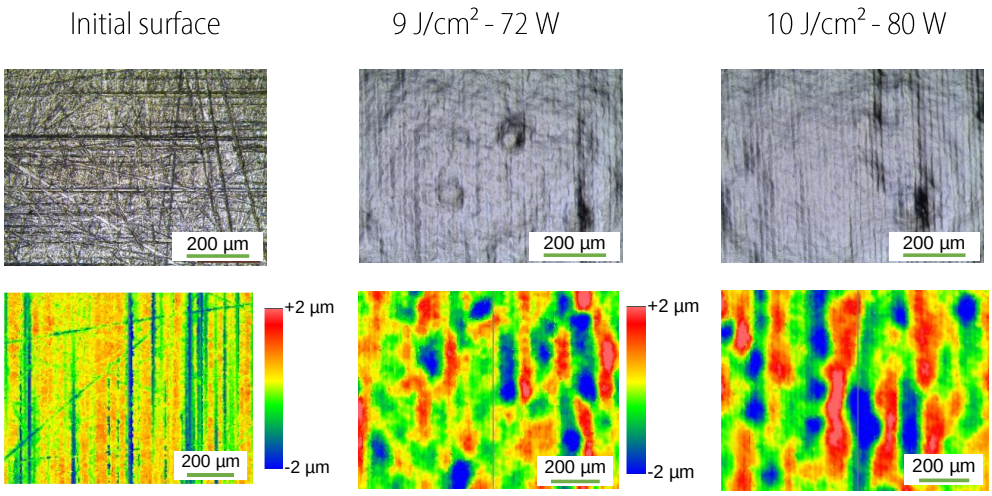

Figure 38: Microscope (up) and WLI (down) pictures for initial surface and 9 and 10 J/cm²

Constant process parameters:
Tool: Q200_TM
dy = 20 µm
v_{scan} = 400 mm/s
n = 1 pass

It is detected that the scratches of the initial surface are smoothed and glossiness is increased when 9 and 10 J/cm² are reached. However, the processed surfaces present some irregularities.

5.2.3 Tool Q400_TM

The tool Q400_TM utilizes the laser beam source TruMicro 7051 and a quadratic fiber so that in combination with an adapted magnification of the zoom a quadratic laser beam focus of 400x400 µm² is realized. The microscope pictures are shown in Figure 39, sharing the same dependency on laser power as the other tools. However, the fluence at which zig zag scratches are smoothed is 4 J/cm², and the highest number of defects is experienced when 6 J/cm² are reached. In addition, for high fluences from 10 - 12 J/cm² the pictures show a border bulging visible at the edges of the track. Border bulging occurs because of part of the molten material being pushed from the center of the melt pool to the edges while laser polishing.

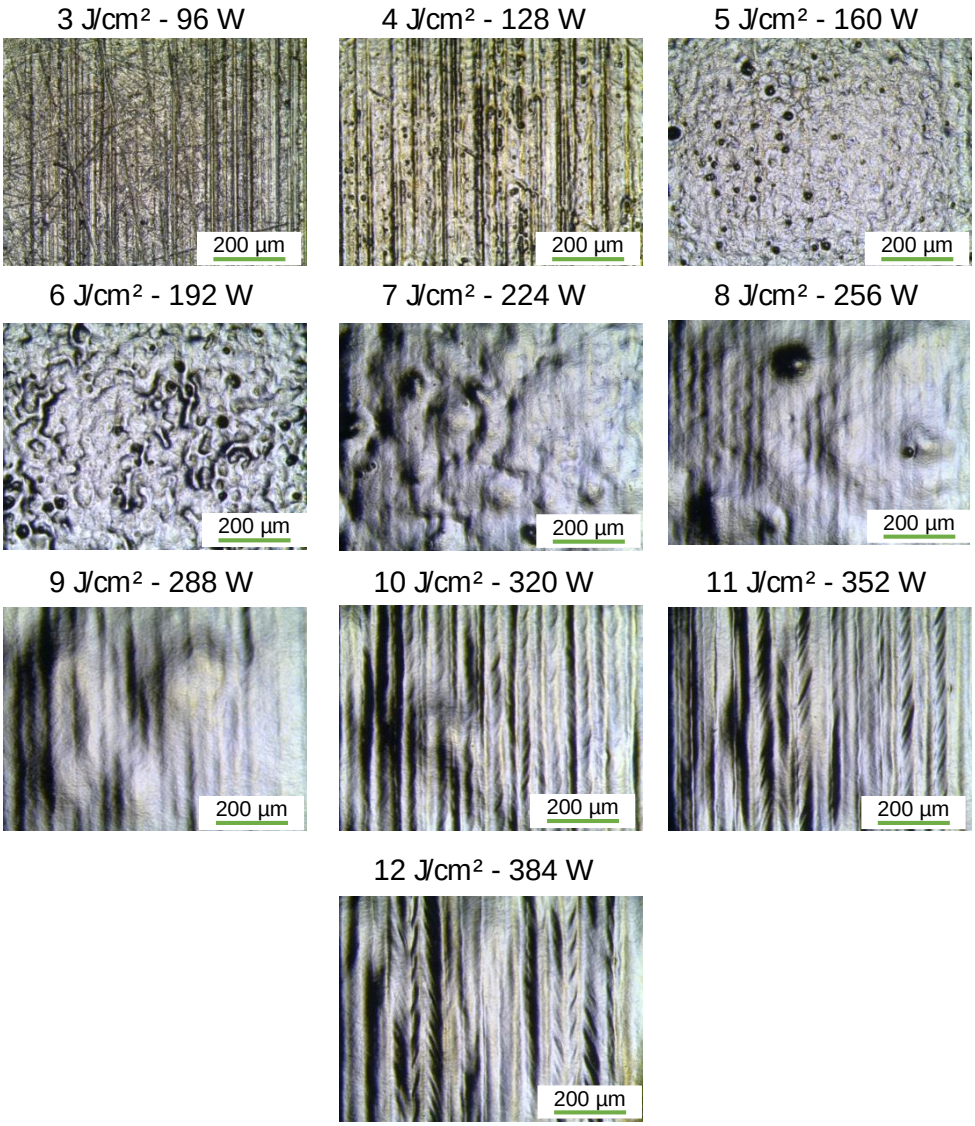

Figure 39:
Microscope pictures of surfaces after laser polishing with different fluences

Constant process parameters:
Tool: Q400_TM
dy = 40 µm
v_{scan} = 800 mm/s
n = 1 pass

The results with regard to the 400x400 µm² laser spot size tool (Q400_TM) are shown in Figure 40, which shows qualitatively the same results as the 200x200 µm² tool: as fluence is increased, roughness below $\lambda = 40$ µm decreases whereas it increases over that spatial wavelength. When 11 and 12 J/cm² are reached, roughness Sa begins to get bigger for $\lambda < 40$ µm.

Figure 40
Sa-spectrum in dependence on fluence

Constant process parameters:
Tool: Q400_TM
dy = 40 µm
v_{scan} = 800 mm/s
n = 1 pass

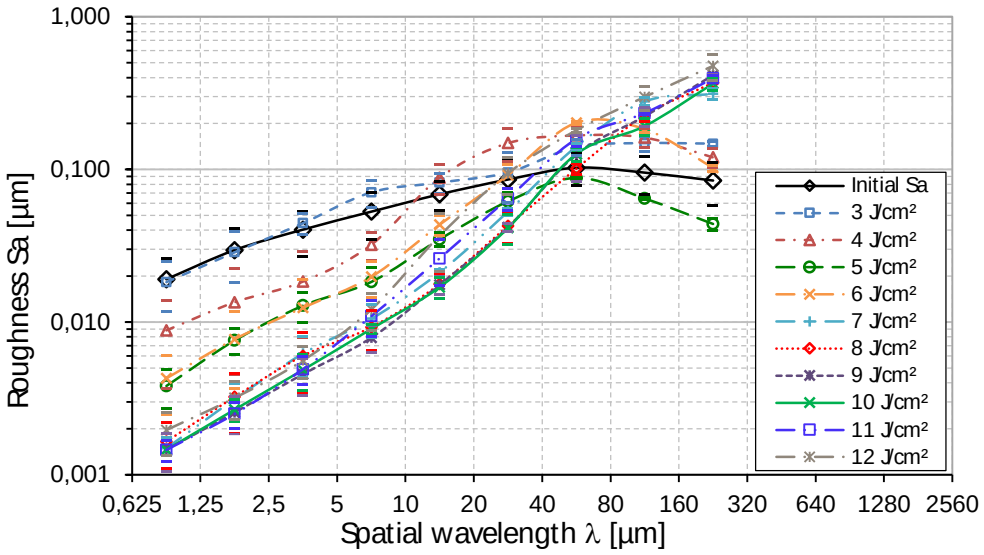

Similarly to what is observed with the Q200_TM tool, fluences ranging from 8 to 10 J/cm² have a similar roughness spectrum. In addition, 9 and 10 J/cm² are the ones that give as a result the smallest micro roughness. Some microscope and WLI pictures are provided for the smallest micro roughness attained (see Figure 41).

Figure 41:
Microscope (up) and WLI (down) pictures for initial surface and 9 and 10 J/cm²

Constant process parameters:
Tool: Q400_TM
dy = 40 µm
v_{scan} = 800 mm/s
n = 1 pass

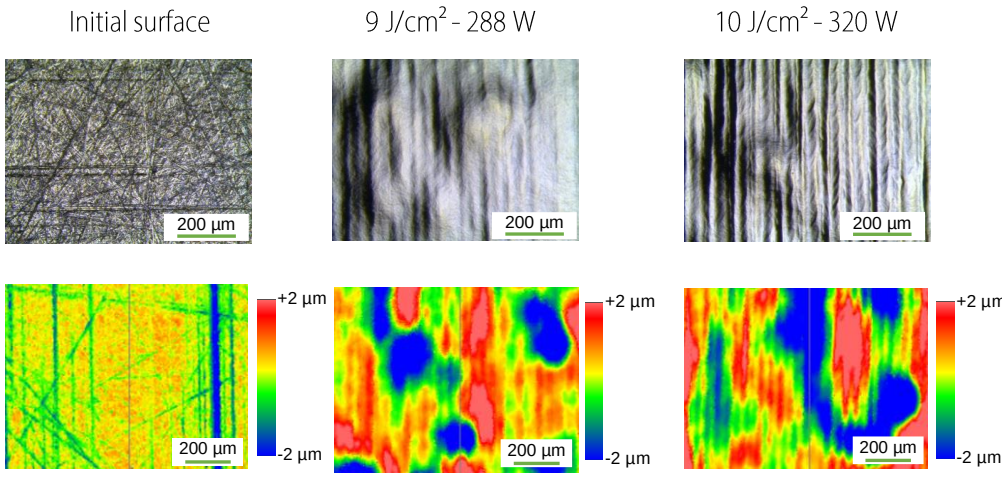

Analogously to the Q200_TM tool, the scratches that the initial surface presented are smoothed when increasing the fluence up to 9 and 10 J/cm², while big irregularities are detected.

5.2.4 Discussion

The three analyzed laser spot sizes pass through the same stages but there are some differences regarding the energy per unit surface that defines the transition between phases. For all tools a fluence is determined that improves the initial roughness spectrum at wavelengths below 40 µm.

The initial surface presents some scratches that are smoothed while fluence is increased. Firstly, the zig zag scratches are smoothed and, at a higher fluence, the grinding marks are also smoothen, value that also results in the highest number of defects after which glossiness is enhanced and the smallest roughness is achieved. Then, if fluence is further increased, the roughness spectrum will get bigger, too. Thus, there are different stages regarding the presence of defects, as shown in Table 7.

Table 7: Overview of the stages regarding the presence of defects for each tool

	Q100_TM	Q200_TM	Q400_TM
Surface is only slightly altered	≤7 J/cm²	3 J/cm²	3 J/cm²
Defects become visible	8 - 11 J/cm²	4 - 10 J/cm²	4 - 10 J/cm²
Defects are no longer visible	≥11 J/cm²	≥11 J/cm²	≥11 J/cm²

It is then observed that the bigger the tool size, the lower the required fluence for removing the initial surface's scratches. This can be due to the fact that bigger tools affect to a bigger surface area, reducing the required fluence to affect the surface. However, this is not completely suitable for the energy per unit surface which gets the smallest roughness. In addition, for bigger tools the last stage with less defects and smaller roughness covers a wider range of fluence. This can be due to preheating phenomena because of the big overlap that is used. A comparison among the smallest roughness spectrums achieved for each tool is shown in Figure 42.

Figure 42:
Sa spectrum in dependence on fluence comparison for the smallest results attained for each tool

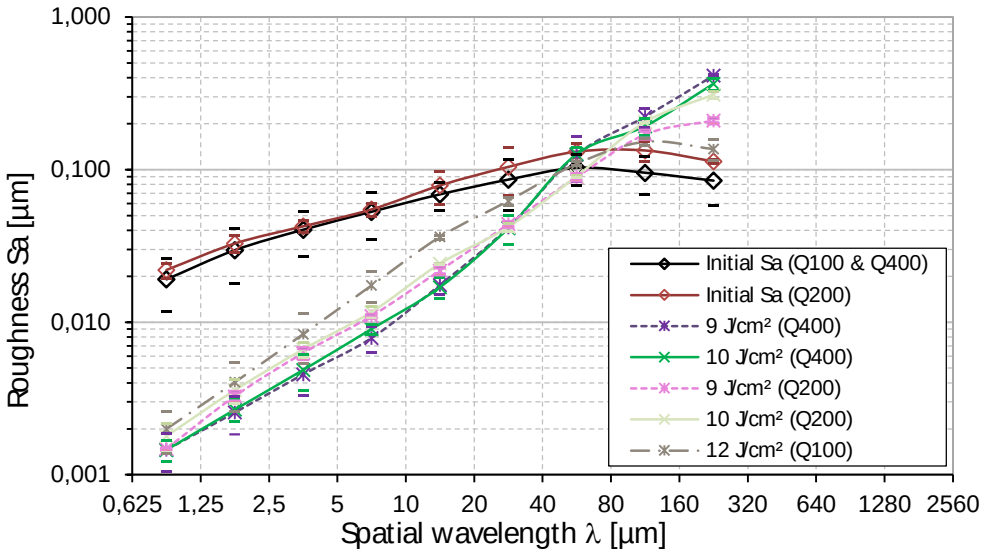

Hence, for all three tools the initial roughness spectrum can be smoothed up to λ = 40 µm. Besides, the smallest micro roughness can be detected for the Q400_TM tool.

When observing the sequence that microscope pictures show, the three of the tools reach a final state where the defects seem to merge and a wave but smooth surface is obtained, where border bulging is appreciated. This is even more visible on the Q400_TM tool's results. In order to clarify this issue, the bulges' size is compared to the laser spot size, which is shown in Figure 43.

Figure 43:
Laser beam's advance along the surface

Constant process parameters:
Tool: Q400_TM
d: pulse to pulse distance
dy = 40 µm
v_{scan} = 800 mm/s
n = 1 pass
Fluence = 12 J/cm²

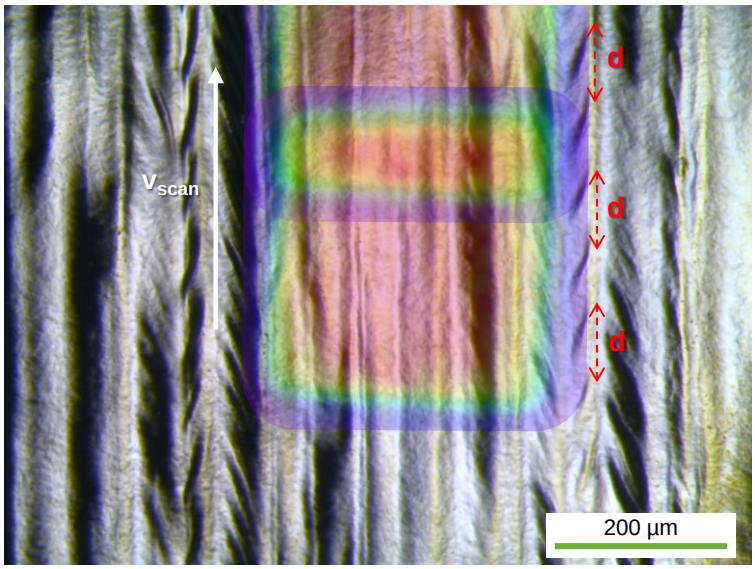

The intensity distribution of the laser beam in the plane of processing is superposed over the processed surface is shown, where d parameter indicates the advance of the laser beam between two pulses. Moreover, the colors of the intensity distribution indicate high (red) and low (blue) intensity, as it was shown in 3.2.1. Hence, the laser spot size fits in the grooves, whose separation distance keeps constant and coincides with pulse to pulse distance, d. Consequently, it is determined that the marks are caused by the single melt pools with a 90% overlap, characteristic of pulsed laser radiation.

Finally, the surfaces processed with the Q200_TM tool and 3 - 6 J/cm² show differences to surfaces processed with a similar fluence but another tool. One possible hypothesis for explaining their unusual results for $\lambda > 80$ µm is the presence of inhomogeneities on the initial surface of the sample, making final roughness lower than initial roughness. This lack of uniformity particularly affects to some of the experiments that were investigated close to the edges of the sample, what applies to the identified unusually low Sa results. Additionally, in this case the initial roughness of the part was investigated on two consecutive fields that might be also affected.

5.3 Surface structuring by laser remelting

For structuring by remelting the TruDisk 1000 is used (Q200_TD tool). The varied process parameters are presented in Table 8. P_M and P_A define the laser power sinusoidal modulation and are determined by the laser power range that corresponds to each v_{scan}. The followed criteria for determining $P_{L\ melt}$ is that the track width is approximately 50% the laser spot size, and the appearance of plasma for $P_{L\ evap}$.

Table 8: Summary of investigated structuring by laser remelting parameters

Structuring by laser remelting investigated parameters			
Laser spot size $d_{L,E}$	200 µm		
Laser power range $P_{L\ melt}$ - $P_{L\ evap.}$	50 - 130 W	60 - 145 W	75 - 175 W
Average laser power P_M	90 W	102.5 W	125 W
Laser power amplitude P_A	40 W	42.5 W	50 W
Scan velocity v_{scan} [mm/s]	50	100	200
Shielding gas	Argon		
Residual oxygen c_{O2}	1000 ppm		
Laser power amplitude P_A investigation			
Structure wavelength λ	1 mm		
Number of passes n	1		
Structure wavelength λ investigation			
Structure wavelength λ	0.5; 1; 1.5; 2 mm		
Number of passes n	1		
Number of passes n investigation			
Structure wavelength λ	1; 2; 3 mm		
Number of passes n	1; 2; 4; 16; 32; 64		
Track overlap investigation			
Structure wavelength λ	1 mm		
Track offset dy	7.8125; 15.625; 31.25;62.5; 125 µm		
Number of passes n	1	1; 2; 4; 8; 16	

Four different experimental investigations are distinguished within the surface structuring by laser remelting part, in which the structure height is presented as a function of the parameters that are indicated below. An overview of the investigation is shown in Table 8. For all investigations that involve a wavelength variation, it is varied as a multiple of an approximately equivalent laser spot

diameter of d_L = 250 µm, which presents a similar surface area as the employed tool. Within the track overlap investigation, both the effects of varying the track offset and the number of passes are analyzed. Track offset is varied from 2^{-1} - 2^{-5} times d_L = 250 µm, while the number of passes ranges from 2^0 - 2^4. Thus, there are two kind of investigations. Along the first investigation all the parameters are constant but the track offset, while both track offset and number of passes are modified on the second one so that the number of remeltings is kept constant.

There are four kinds of investigations within this part:

- Influence of laser power amplitude on structure height (single tracks)
- Influence of scanning velocity and wavelength on structure height (single tracks)
- Influence of number of repetitions on structure height (single tracks)
- Influence of track overlap on structure height (extensive structuring)

5.3.1 Laser power amplitude

After determining average laser power and laser power amplitude for each scan velocity, the P_A is systematically decreased in 5 W steps. In Figure 44 the measured structure height is shown in dependence on the laser power amplitude. For all three scan velocities an approximately linear dependency of structure height on laser power amplitude is observed. Besides, higher structures are attained with 50 and 100 mm/s, whereas lower structures are originated when increasing scan velocity up to 200 mm/s.

Figure 44:
Structure height in dependence on laser power amplitude for different scan velocities

Constant process parameters:
Tool: Q200_TD
dy = 800 µm
n = 1 pass
λ = 1 mm

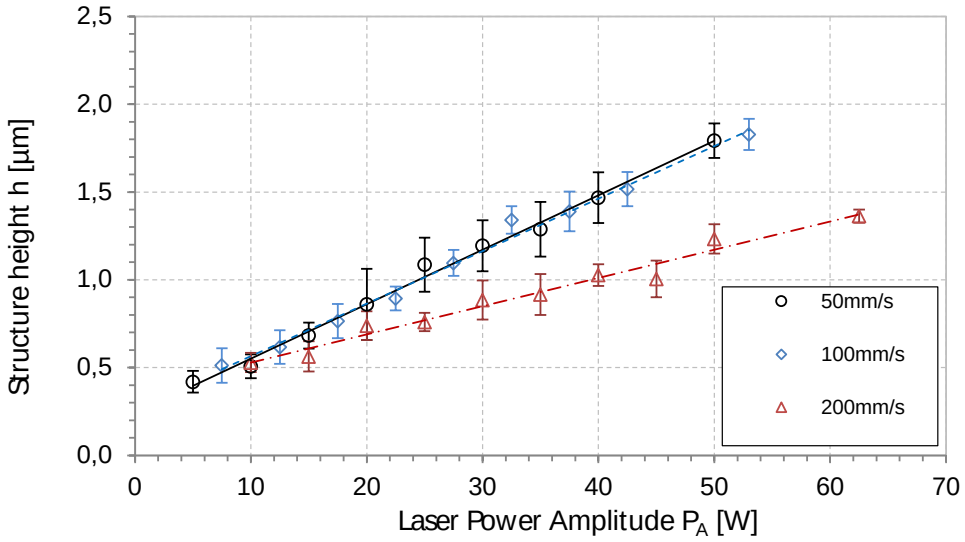

Thus, the greatest height of $h = 1.83 \pm 0.09$ µm is attained for 100 mm/s, $P_M = 102.5$ W and $P_A = 53$ W.

5.3.2 Scanning velocity and wavelength

The influence of wavelength on structure height is studied by varying λ as two, four, six and eight times $d_L = 250$ µm, obtaining the results shown in Figure 45 for the three scan velocities investigated.

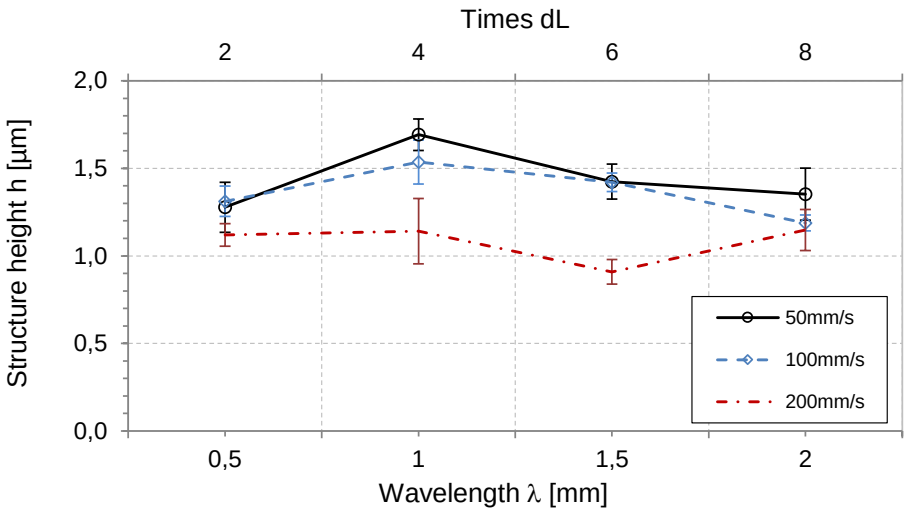

Figure 45: Structure height in dependence on wavelength for different scan velocities

Constant process parameters:
Tool: Q200_TD
dy = 800 µm
n = 1 pass

In this case, the maximum structure height, h = 1.69 ± 0.09 µm, is achieved with 50 mm/s scan velocity and $\lambda = 1$ mm and decreases to h ≈ 1.35 µm at $\lambda = 2$ mm, giving rise to the kind of structures shown in Figure 46.

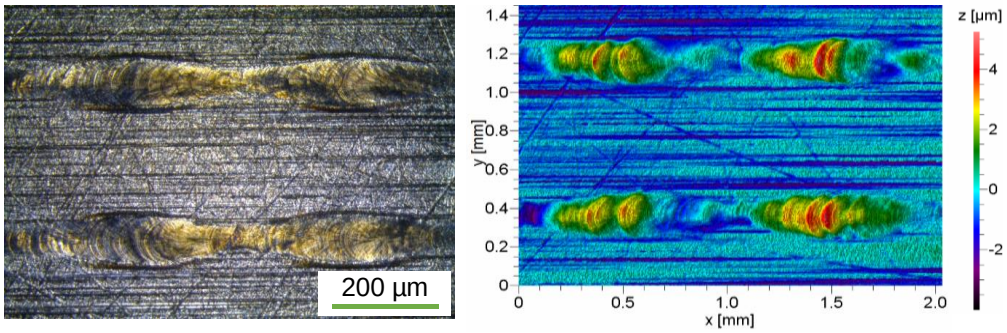

Figure 46: Microscope (left) and WLI (right) pictures after structuring by remelting with v_{scan} = 50 mm/s λ = 1 mm

In addition, the biggest structures with 100 mm/s are also attained at $\lambda = 1$ mm, reaching a height of h = 1.54 ± 0.13 µm, and decrease for bigger wavelengths. However, and in an analogue way to the previously explained experiment, using a scanning velocity of v_{scan} = 200 mm/s results in smaller structure heights. The local maximum is detected for structures with a wavelength of $\lambda = 1$ mm, matching with four times the d_L.

5.3.3 Number of repetitions

In order to achieve greater structure heights, the effect of increasing the number of passes for different wavelengths is investigated. The number of repetitions is varied

from 2^0 up to 2^6 at structure wavelengths of four, eight and twelve times the laser beam diameter d_L = 250 µm.

The results shown in Figure 48 represent the achieved structure heights for v_{scan} = 100 mm/s and three different wavelengths. Every additional number of repetitions significantly increase the structure height up to 16 or 32 passes, where a saturation is reached. This occurs independently of the wavelength, and also applies to v_{scan} = 200 mm/s.

Figure 47:
Structure height in dependence on number of repetitions for different wavelengths

Constant process parameters:
Tool: Q200_TD
dy = 800 µm
v_{scan} = 100 mm/s

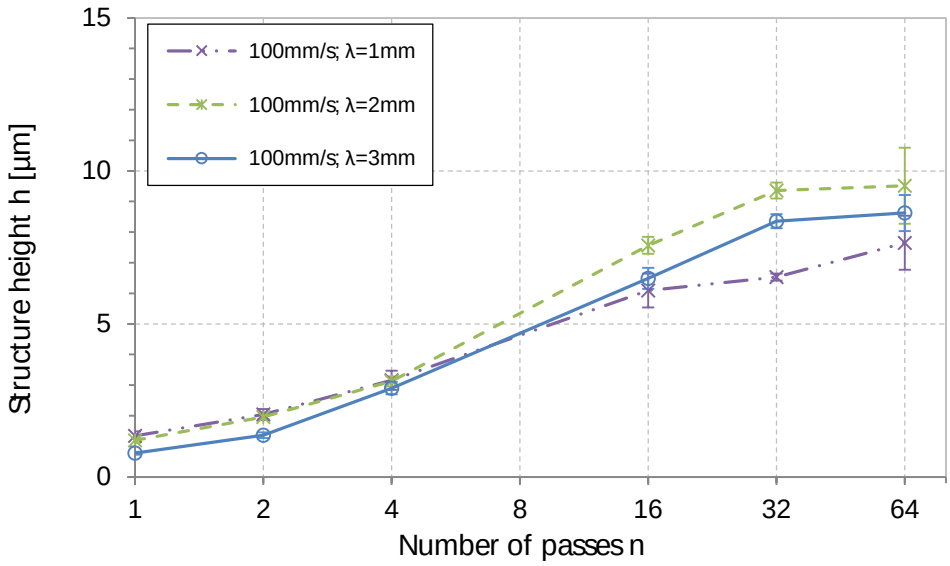

However, by comparing the performance of the three scan velocities for the same wavelength, it is observed that processing with v_{scan} = 50 mm/s does not show the same saturation of structure height for a greater number of repetitions. The structure height continues to increase up to 64 passes reaching h = 15.66 ± 0.64 µm, as it is shown in Figure 48.

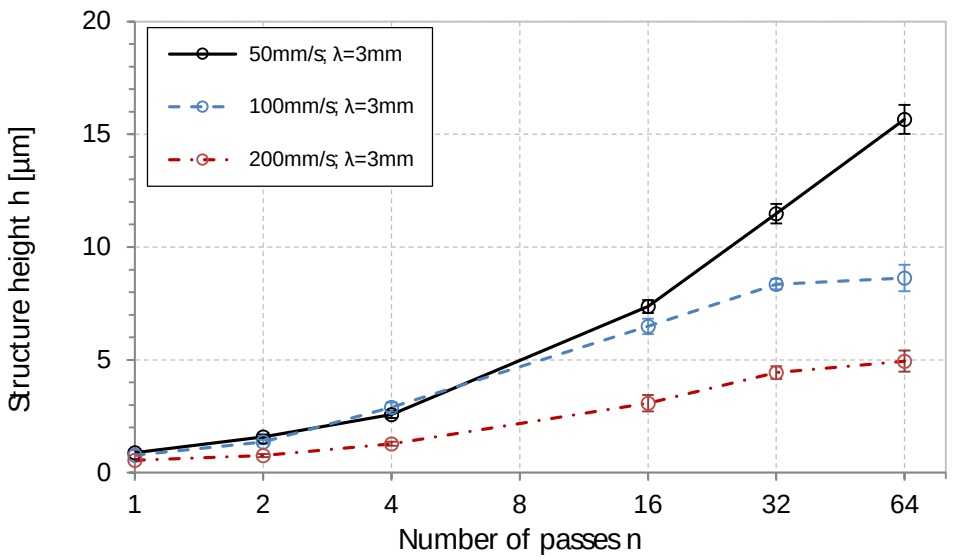

Figure 48: Structure height in dependence on number of repetitions for different scan velocities

Constant process parameters:
Tool: Q200_TD
dy = 800 µm
λ = 3 mm

All the above mentioned applies to the other two investigated wavelengths, 1 mm and 2 mm. Besides, the structure heights attained with λ = 2 mm are similar to the ones obtained with λ = 3 mm. However, using λ = 1 mm shows smaller structure heights, having a maximum height of 11.42 ± 0.54 µm. (see Figure 63 (10.4 - Appendix)

The highest structures are always achieved with v_{scan} = 50 mm/s and λ > 4*d_L = 1 mm. The increase in structure height is exemplarily shown for v_{scan} = 50 mm/s and λ = 3 mm in Figure 49, where it is detected that the higher the number of passes, the bigger the structures.

Figure 49:
Evolution of the structure with increasing number of passes.

Constant process parameters:
Tool: Q200_TD
dy = 800 µm
v_{scan} = 50 mm/s
λ = 3 mm

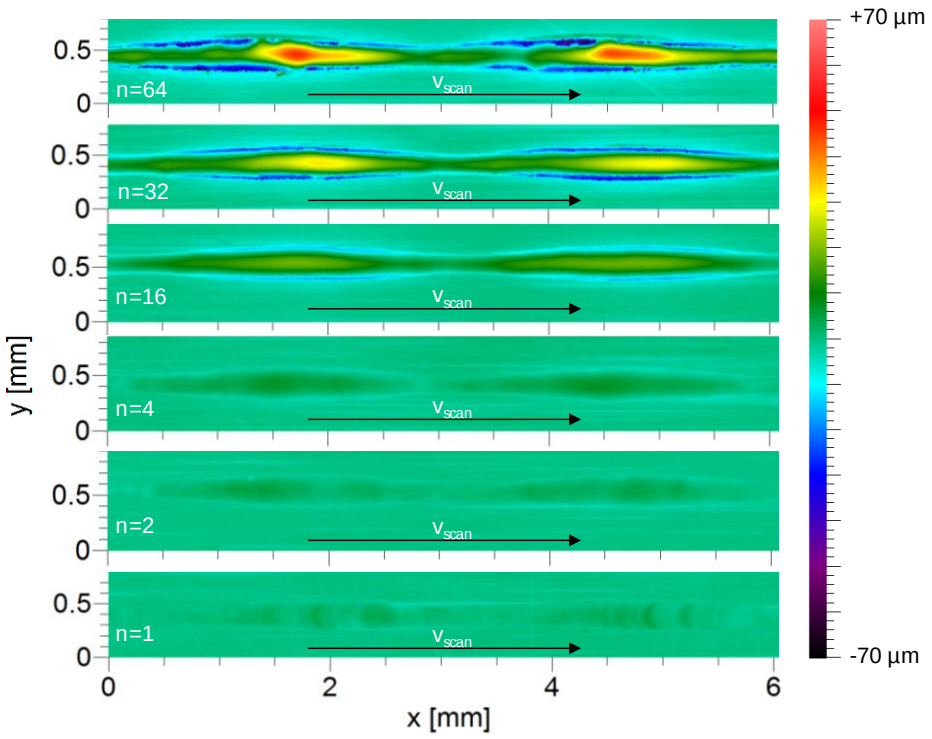

Furthermore, in Figure 50 both longitudinal section and FFT are shown for each investigated number of passes, so that the effects of increasing the number of passes are better appreciated.

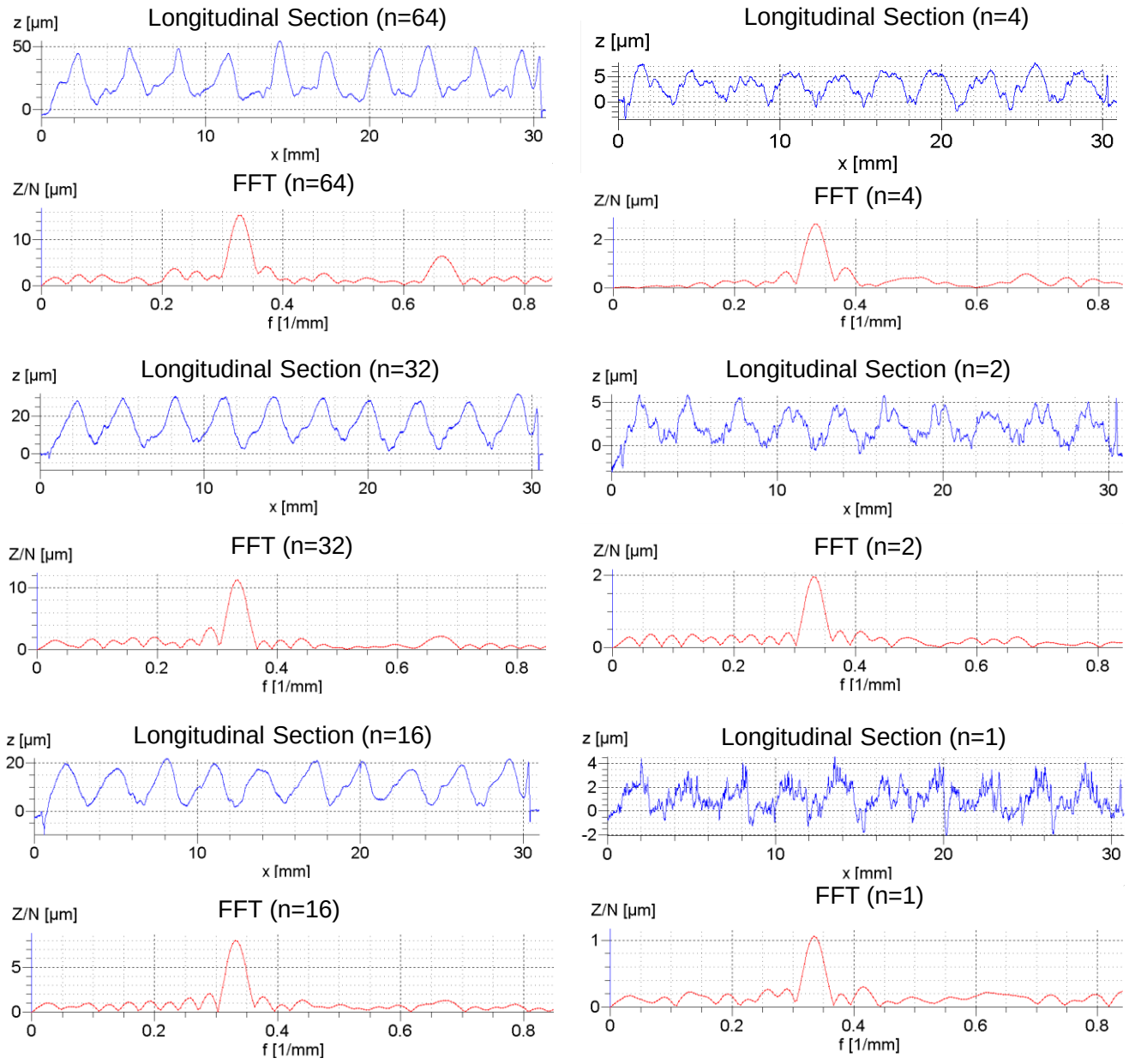

Figure 50: Longitudinal sections and Fourier analyses (FFT) for increasing number of passes. Constant process parameters: Tool: Q200_TD; dy = 800 µm; v_{scan} = 50 mm/s; λ = 3 mm

The longitudinal section, that shows the sinusoidal modulation, gets more stable as the number of passes is increased. Moreover, the Fast Fourier Transform (FFT) presents a peak at a frequency of approx. 0.333 mm^{-1}, which is the inverse of the employed wavelength.

5.3.4 Track overlap

In this case, the influence of track offset on structure height for an extensive structuring is investigated. The track offset is varied from 2^{-1} to 2^{-5} times the laser beam diameter d_L = 250 µm, obtaining the smallest height with the biggest track offset of dy = 125 µm. The resulting structure height in dependence on track offset for three different scanning velocities is shown in Figure 51.

Figure 51: Structure height in dependence on track offset for different scan velocities

Constant process parameters:
Tool: Q200_TD
λ = 1 mm

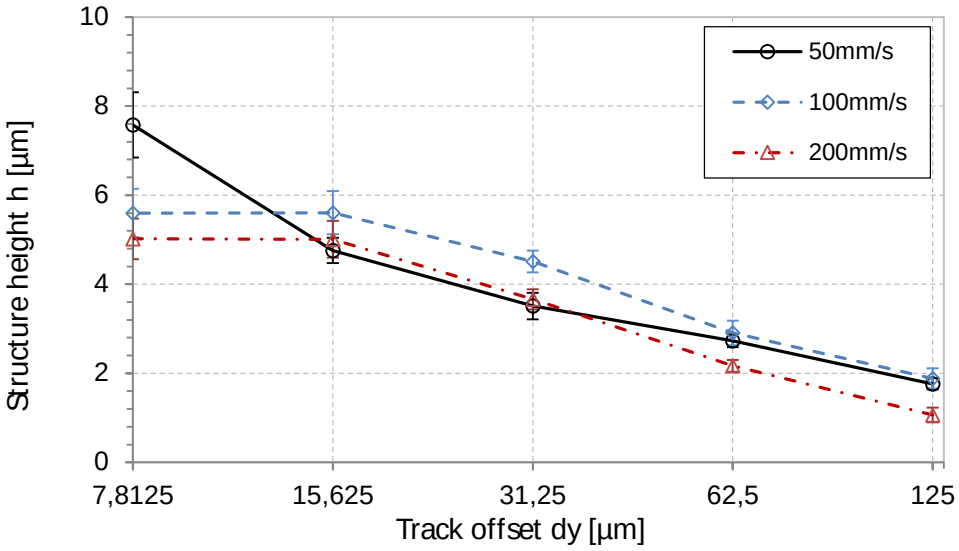

Greater structure heights are attained with smaller track offsets. For scan velocities of 100 and 200 mm/s, track offset reductions under 15.63 µm do not increase the structure height. In this investigation, the highest structures are achieved with v_{scan} = 50 mm/s at dy ≈ 8 µm, reaching h = 7.58 ± 0.73 µm for structuring with one pass.

In the following, the results for structure height are presented as a function of the processing time instead of the track offset. This way of representing allows comparing how the employment of each scan velocity affects structure height for the same processing time and is defined as

5.1

$$t_{process} = n * \frac{l_x * l_y}{v_{scan} * dy}$$

where l_x and l_y are defined as the structured field's size.

According to the formula, the smaller the track offset, the greater the structures that are achieved, but also processing time increases. Given the graph in Figure 52,

where the structure height is shown in dependence on processing time, for the same processing time, higher scan velocities result in higher structures until saturation is reached (λ = 1 mm).

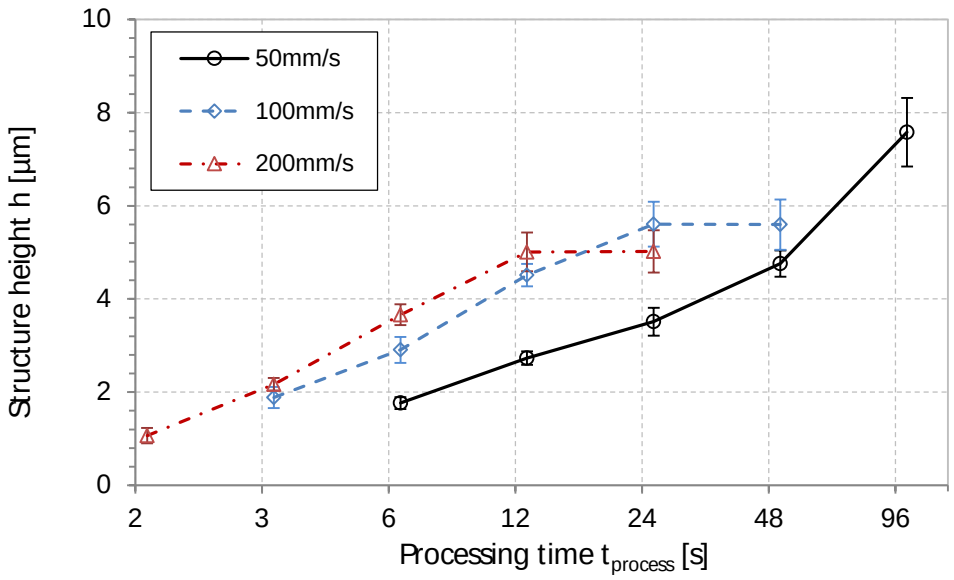

Figure 52: Structure height in dependence on processing time for different scan velocities

Constant process parameters:
Tool: Q200_TD
λ = 1 mm

Furthermore, the results concerning a simultaneous variation of both the number of passes and track offset are presented in Figure 53. The number of remeltings, n_u, is kept constant at 32 remeltings within this part of the investigation. This parameter is defined as

5.2

$$n_u = n * \frac{d_L}{dy}$$

Then, both the track offset and number of overall passes are adapted so that the number of remeltings is constant.

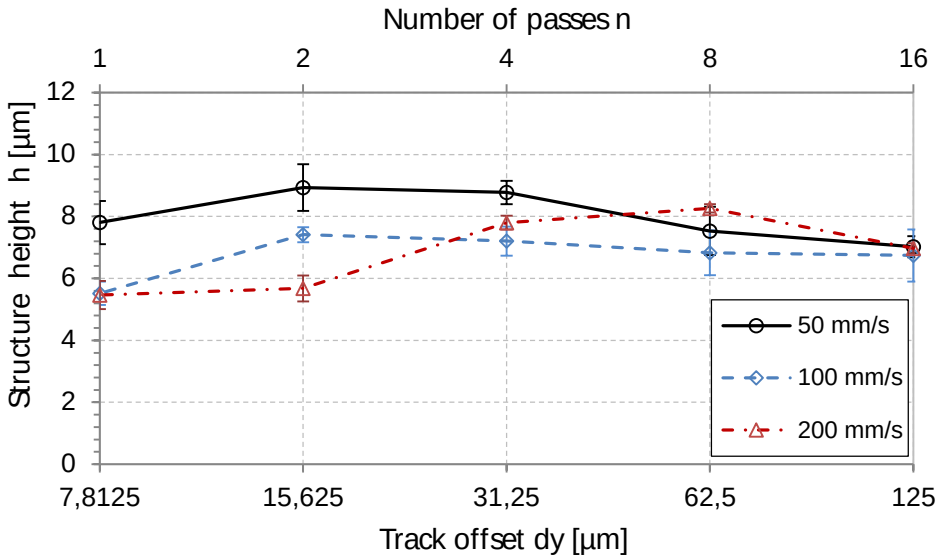

Figure 53:
Structure height in dependence on track offset and number of passes for different scan velocities

Constant process parameters:
Tool: Q200_TD
λ = 1 mm

According to the graph shown in Figure 53, for a constant number of remeltings the three scan velocities give similar results, especially from dy = 15.63 µm onwards.

5.3.5 Discussion

According to the different developed investigations, several conclusions are reached. The results show a linearity of laser power amplitude and structure height, then, as laser power amplitude is increased, greater structures are achieved. In addition, a structure height local maximum is detected for wavelengths of four times the laser spot diameter.

The results regarding the variation of the number of passes for different wavelength values show that every additional number of passes significantly increases the structure height. However, especially greater structures are attained for wavelengths bigger than four times the laser spot diameter. Moreover, processing with 100 and 200 mm/s implies a saturation state for all the investigated wavelengths, involving that the structures stop growing after 16 passes, approximately.

Finally and according the two investigations with regard to the track overlap variation, it is concluded that the structures are higher as the track offset is decreased, that is, as the track overlap or number of remeltings is increased. For scan velocities of 100 and 200 mm/s, a saturation point for structure height is reached so that track offset reductions under 15.63 µm do not increase the structure

height. In addition, for a constant number of remeltings dy = 15.63 µm also marks the track offset where saturation starts. By selecting the correct laser power (average and amplitude), combined with an adapted set of parameters (number of passes and track offset), it is concluded that 200 mm/s scan velocity can be used and give similar results as 50 mm/s. Furthermore, increasing the scan velocity implies a lower processing time, which opens the possibility to increase the number of passes and/or decrease the track offset in order to achieve even greater structure heights than with 50 mm/s.

6 Summary

The results presented in this master thesis where achieved within the DFG-funded priority program SPP 1676 "Dry Metal Forming". The aim of this priority program is the development of sustainable production technologies for dry processing in metal forming, which implies the avoidance of lubricant. This approach brings several benefits affecting on, for instance, economical or environmental aspects. One strategy for realizing dry metal forming is the modification of the tool's surface by laser macro and micro polishing and surface structuring by laser remelting. The objective of this thesis is the development of process parameters and the analysis and characterization of the produced surfaces. The investigation is done on 1.2379+ cold work steel samples. The process parameters have been systematically varied in order to determine the performance of the material and characterize the produced surface concerning spectral surface roughness or structure height. Besides, the relation between the process parameters and the wavelengths of the roughness spectrum has also been analyzed.

With macro polishing, as laser power is increased the roughness is lowered for all spatial wavelengths up to 160 µm as long as no oxidation appears. With regard to the $d_{L,E}$ = 100 µm tool, an increasing scan velocity leads to a smaller roughness for spatial wavelengths up to 160 µm, while this reduction of surface roughness is limited to spatial wavelengths of 10 µm for the $d_{L,E}$ = 200 µm tool. Furthermore, an increasing number of passes (up to four) does not automatically lead to a reduction of roughness that could not be achieved as well with a smaller number of passes and adapted laser power. Macro polishing using one or two passes leads to the best overall improvement of the roughness spectrums for both tools. The process of micro polishing smoothens roughness up to a spatial wavelength of 40 µm. In addition, increasing the size of the laser beam or the fluence results in a reduction of roughness for the whole spectrum of spatial wavelengths. Compared to the best spectral surface roughness achieved by using macro polishing, micro polishing decreases the surface roughness significantly, especially for spatial wavelengths below 10 µm.

The experimental investigations for structuring by laser remelting show that structure height depends almost linearly on laser power amplitude. Greater structure heights are achieved for $\lambda = 4*d_L = 1$ mm. Moreover, there is a significant rise in structure height, for wavelengths $\lambda > 4*d_L = 1$ mm as the number of passes are increased, being this dependence not linear. However, there seems to be a maximal number of passes after which the structure height get saturated and stops increasing further. The variation of the track offset leads to a similar result where this saturation of structure height is observed for small track offsets. However, when varying both number of passes and track offset for an established processing

time, it is concluded that structure height is increased for greater scan velocities and a greater number of passes than for a small number of passes, small track offsets and small scan velocities.

7 Outlook

As far as macro polishing is concerned, two laser spot sizes are studied, for which three scan velocities in combination with three different numbers of passes are investigated. Since the higher the scan velocity, the lower the measured roughness, future investigations could include the investigation of higher scan velocities, so that it could be determined whether a smaller roughness can be accomplished. However, no increase in laser beam size nor in number of passes seems to improve present results a priori.

Micro polishing is studied with three laser spot sizes. In this case, investigating bigger tools can be object of interest, since smallest roughness is attained with the biggest laser beam size investigated. However, this would probably involve preheating, as discussed above. Thus, increasing the pulse offset could be a way to rise the processing rate and decrease the preheating effects.

With regard to structuring by remelting, the influence of the track overlap needs to be analyzed by varying track offset in combination with the number of passes. Thus, the optimum set of parameters could be determined and therefore investigate the performance for scan velocities greater than 200 mm/s.

Additionally, future investigations could thus involve topics such as the reproducibility of the presented results, the combination of macro and micro polishing. Finally, the development of wear investigations conforms another prospective line so that the influence of laser polishing and surface structure by laser remelting on the wear behavior is characterized.

8 References

[1] Xing Lu; Cunsheng Zhang; Guoqun Zhao; Yanjin Guan; Liang Chen; Anjiang Gao, Erratum to "State-of-the-art of extrusion welding and proposal of a method to evaluate quantitatively welding quality during three-dimensional extrusion process". Materials & Design, 2016; 90: 1251.

[2] Dong-Hwan Jang; Tae-Kon Ryou; Dae-Young Yoon; Beong-Bok Hwang, Erratum to "The process sequence design of a power-assisted steering part". Journal of Materials Processing Technology, 2001; 116: 310-316.

[3] F. Vollertsen; F. Schmidt, "Dry Metal Forming: Definition, Chances and Challenges". International Journal Precision Engineering and Manufacturing - Green Technology 1/1, 2014: 59-62

[4] E. V. Bordatchev; A. Hafiz; O. Tutunea-Fatan, "Performance of Laser Polishing in Finishing of Metallic Surfaces". International Journal of Advanced Manufacturing Technology, 2014; 73: 35-52.

[5] C. Nüsser; J. Kummstel; T. Kiedrowski; A. Diatlov; E. Willenborg, "Process- and Material- Induced Surface Structures During Laser Polishing". Advanced Engineering Materials, 2015; 17: 268-277.

[6] O. Blomster; M. Blomqvist, "Square Formed Fiber Optics for High Power Applications". In Proceedings of the Fourth International WLT - Conference on Lasers in Manufacturing, Munich, 2007.

[7] Fujikura, "Square Core Fibre", [Online]. Available: http://www.fujikura.co.uk/products/medical-industrial-optical-fibre/square-core-fibre/#productDescription. [Accessed 06.07.2016]

[8] Photonics, "Square Fibers Solve Multiple Application Challenges", [Online]. Available: http://www.photonics.com/Article.aspx?AID = 45913. [Accessed 06.07.2016]

[9] C. Nüsser; I. Wehrmann; E. Willenborg, "Influence of Intensity Distribution and Pulse Duration on Laser Micro Polishing", Physics Procedia 2011; 12.

[10] Primes, „MSM Datasheet", [Online]. Available: http://www.primes.de/en/products/beam-distribution/focus-measurement/microspotmonitor-msm.html. [Accessed 05.07.2016]

[11] Dörrenberg Edelstahl, "1.2379PLUS Datasheet", [Online]. Available: http://www.doerrenberg.de/uploads/tx_c1x1downloads/1.2379PLUS_en.pdf. [Accessed 05.07.2016]

[12] Leica Microsystems, "Stereo Microscope with a Difference Leica M205C", [Online]. Available: http://www.leica-microsystems.com/products/stereo-microscopes-macroscopes/research-manual/details/product/leica-m205-c/. [Accessed 06.07.2016]

[13] Zygo, "NewView 7300 Specifications Sheet", [Online]. Available: https://www.google.de/url?sa = t&rct = j&q = &esrc = s&source = web&cd = 1&cad = rja&uact = 8&ved = 0ahUKEwihwqSa697NAhWLthQKHQ04AL8QFggcMAA&url = http%3A%2F%2F83.169.23.21%2Ffiles%2Fdownloads%2Fzygo%2Ffr%2Fzygo_newview7300spec_fr01.pdf&usg = AFQjCNFYCyUZqUPI21IUFPYx9EQrb26ycQ&sig2 = I9XsY2g1R3-QzcOE7qc38w&bvm = bv.126130881,d.d24. [Accessed 06.07.2016]

[14] E. Willenborg, "Polieren von Werkzeugstählen mit Laserstrahlung". Dissertation, RWTH Aachen University, 2006.

[15] A. Temmler, "Laserumschmelzstrukturierung". Ph.D. Thesis, RWTH Aachen University, 2012.

9 Symbols and Abbreviations

α	Angle between beam's energy distribution's edge and machine's axis
β	Angle of incidence
b_{track}	Width of track
c_{O_2}	Residual oxygen
cw	Continuous wave
d	Pulse to pulse distance
$d_{L,E}$	Laser spot edge length
d_L	Laser spot diameter
dy	Track offset
EDM	Electrical Discharge Machining
FFT	Fast Fourier transform
f_p	Pulse frequency
h	Structure height
ILT	Fraunhofer Institute for Laser Technology
λ	Wavelength
λ_{em}	Emitting laser wavelength
lc	Cut-off length
l_s	Scan Vector Length

Lt	Traverse length
l_x	Test field's X dimension
l_y	Test field's Y dimension
MSM	MicroSpotMonitor
n	Number of passes
NC	Numeric control
P_A	Laser power amplitude
P_L	Laser power
$P_{L\ evap.}$	Maximum laser power after which material evaporates
$P_{L\ melt}$	Minimum laser power required to start remelting
$P_{L\ Min}$	Minimum laser power
$P_{L\ Max}$	Maximum laser power
P_M	Average laser power
Q100_TD	100x100 µm² laser spot size TruDisk tool
Q200_TD	200x200 µm² laser spot size TruDisk tool
Q100_TM	100x100 µm² laser spot size TruDisk tool
Q200_TM	200x200 µm² laser spot size TruMicro tool
Q400_TM	400x400 µm² laser spot size TruMicro tool
Ra	Mean roughness
Sa	Roughness spectrum

t_p	Pulse duration
$t_{process}$	Processing time
v_{scan}	Scan velocity
WLI	White light interferometer

10 Appendix

10.1 Tool's caustic beams

Figure 54:
Caustic beams for
a) 100x100 µm²
b) 200x200 µm²
c) 400x400 µm² laser spot size tools.

a)

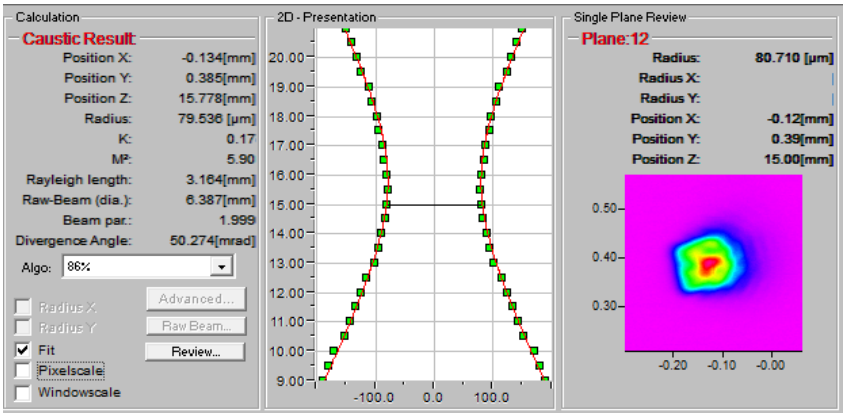

b)

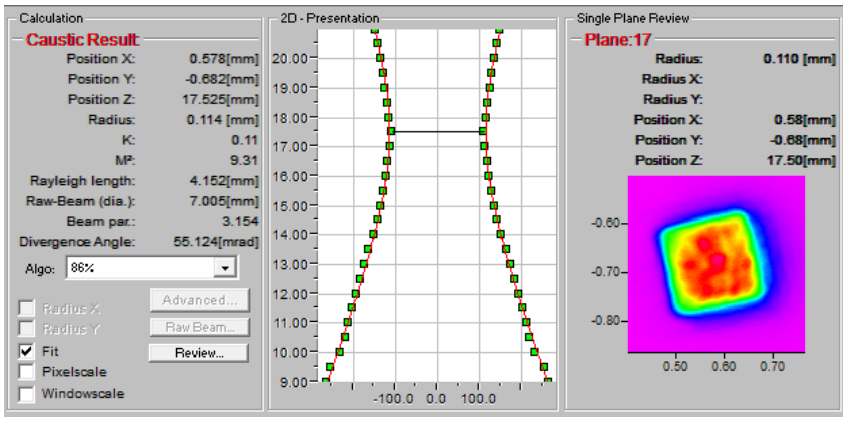

c)

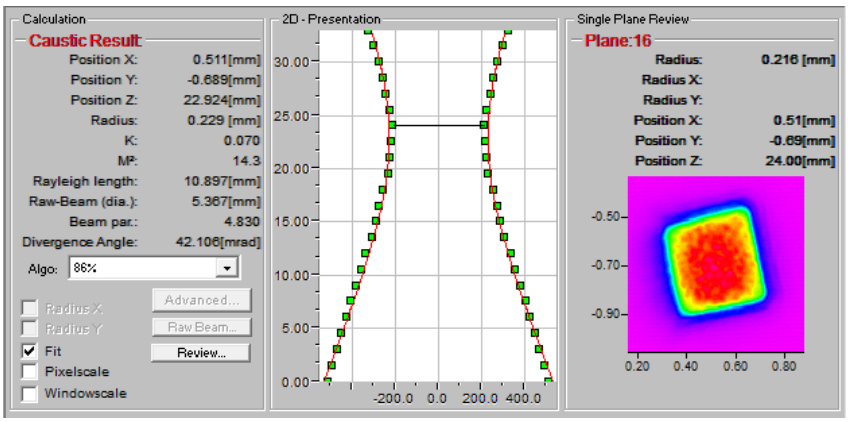

10.2 Macro polishing

- 100x100 µm² laser spot size tool:

Figure 55:
Roughness Ra in dependence on laser power for different number of passes

Constant process parameters:
Tool: Q100_TD
dy = 20 µm
a) v_{scan} = 50 mm/s
b) v_{scan} = 100 mm/s

a)

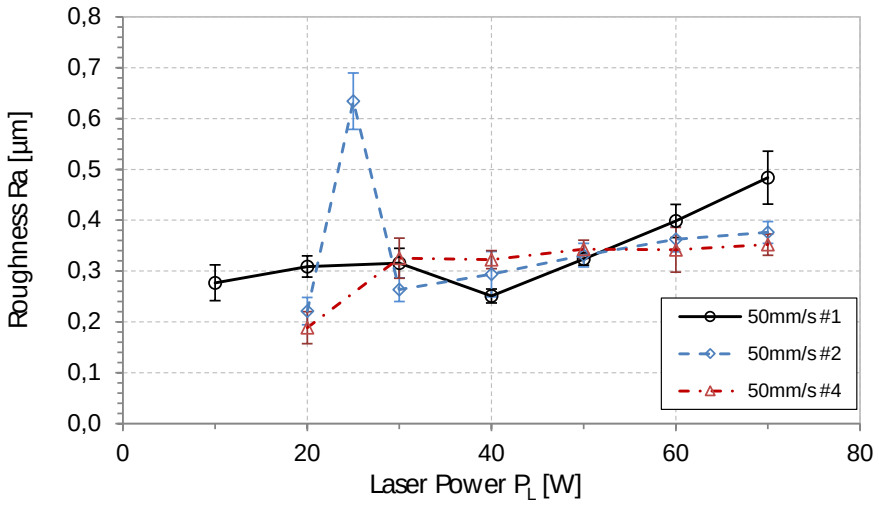

b)

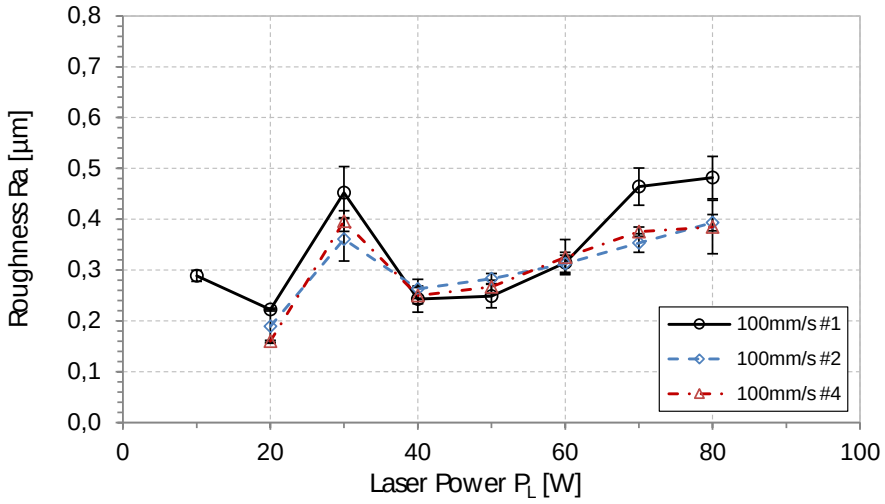

Figure 56:
Sa-spectrum in dependence on laser power

Constant process parameters:
Tool: Q100_TD
dy = 20 µm
v_{scan} = 50 mm/s
a) n = 1 pass
b) n = 2 passes
c) n = 4 passes

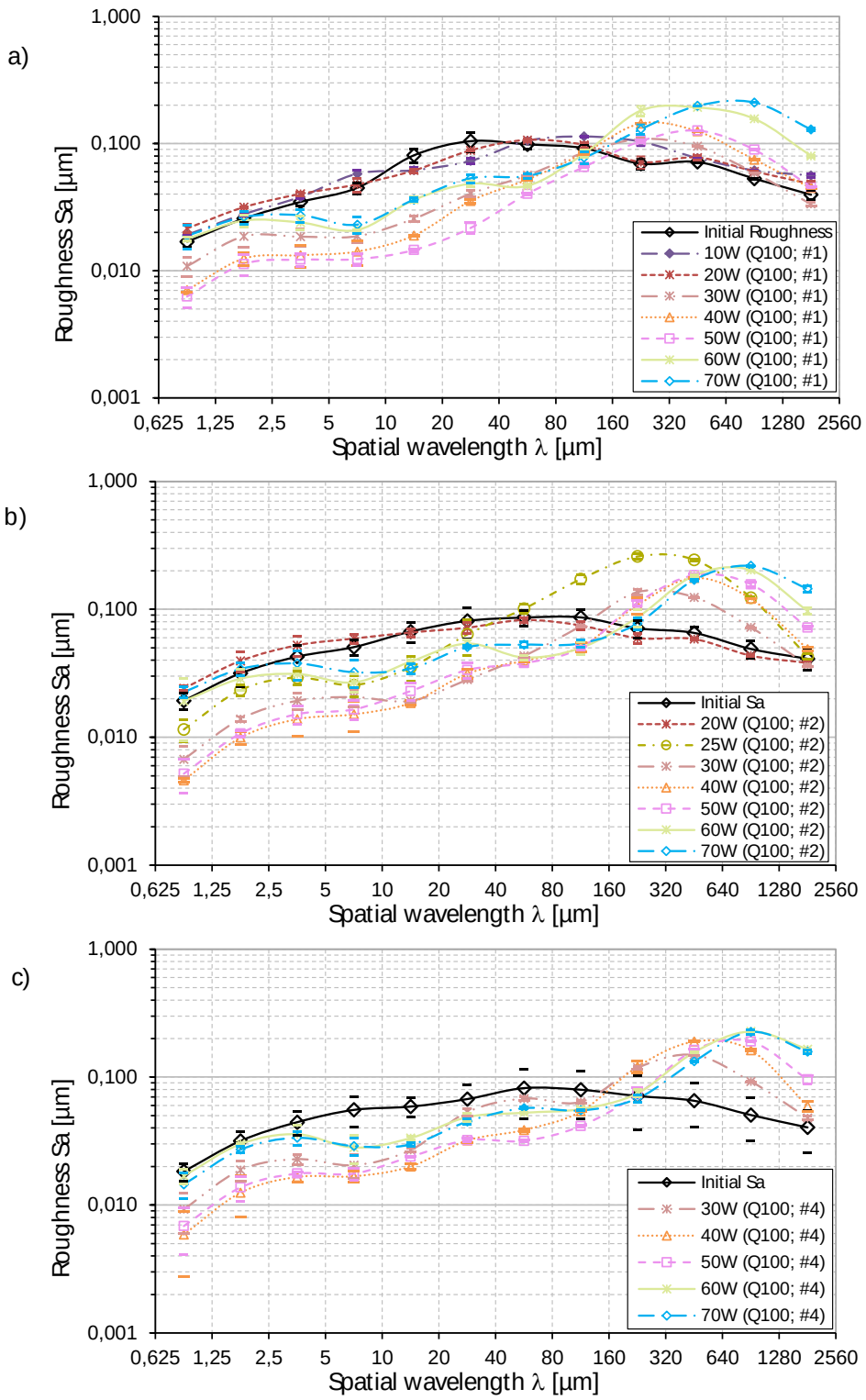

Figure 57:
Sa-spectrum in dependence on laser power

Constant process parameters:
Tool: Q100_TD
dy = 20 µm
v_{scan} = 100 mm/s
a) n = 1 pass
b) n = 2 passes
c) n = 4 passes

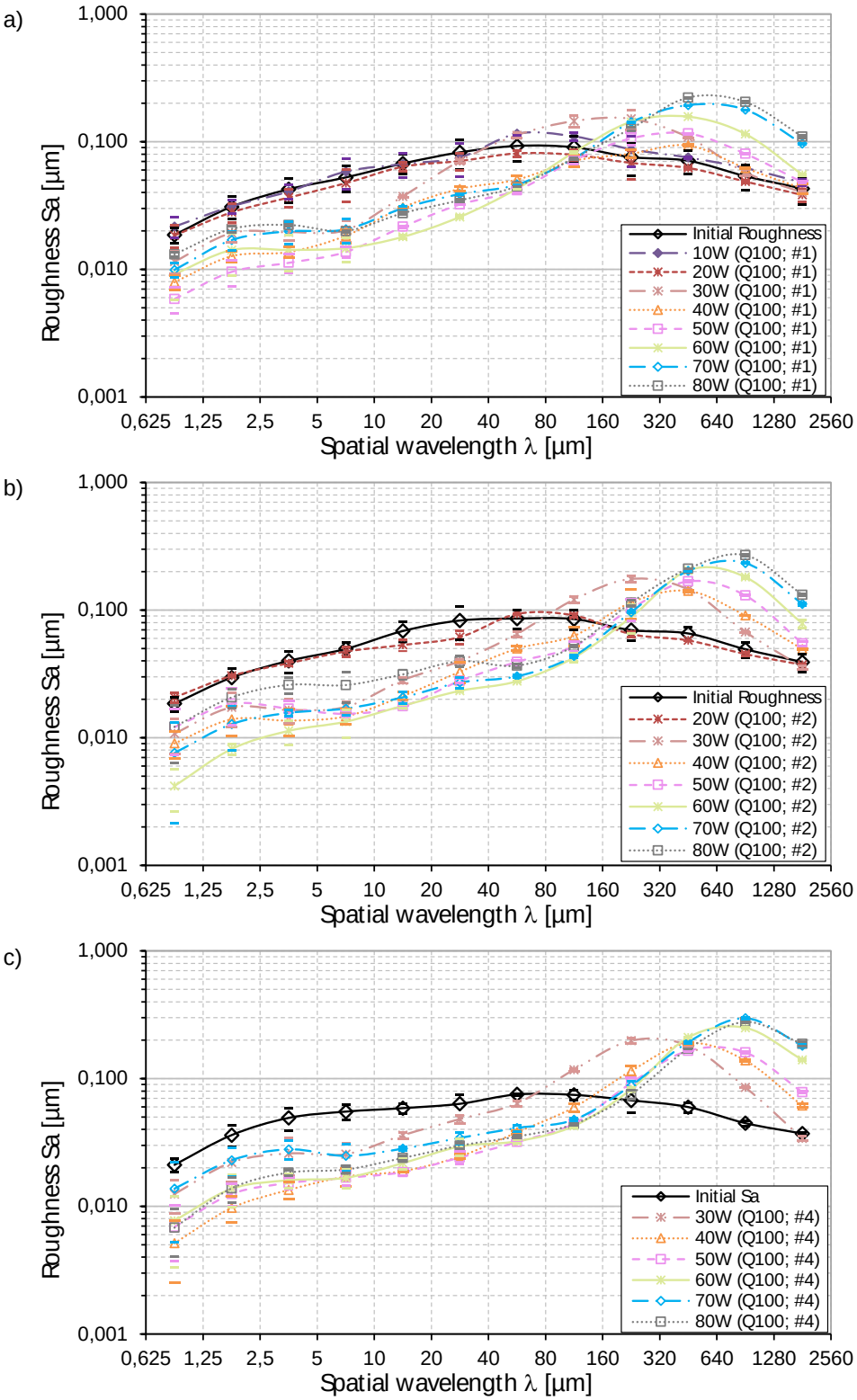

Figure 58:
Sa-spectrum in dependence on laser power

Constant process parameters:
Tool: Q100_TD
dy = 20 µm
v_{scan} = 200 mm/s
a) n = 1 pass
b) n = 4 passes

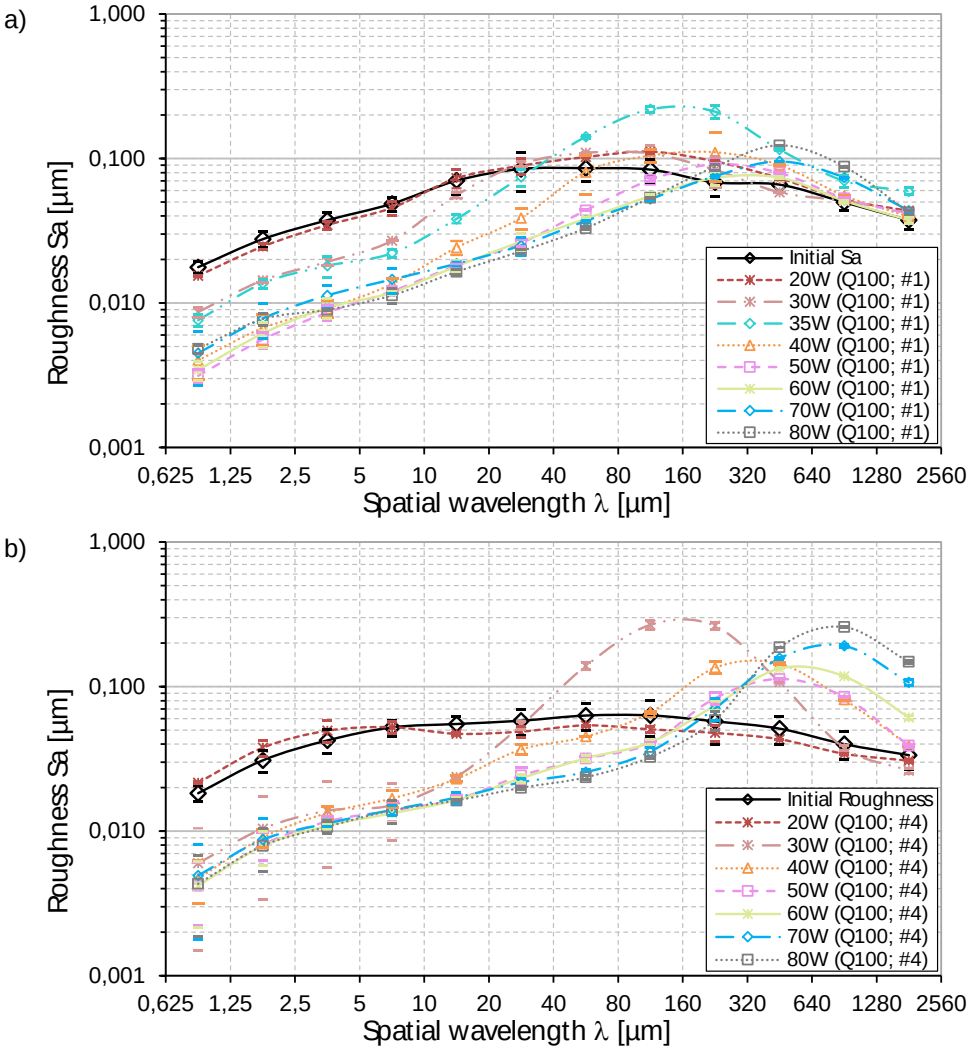

- 200x200 µm² laser spot size tool:

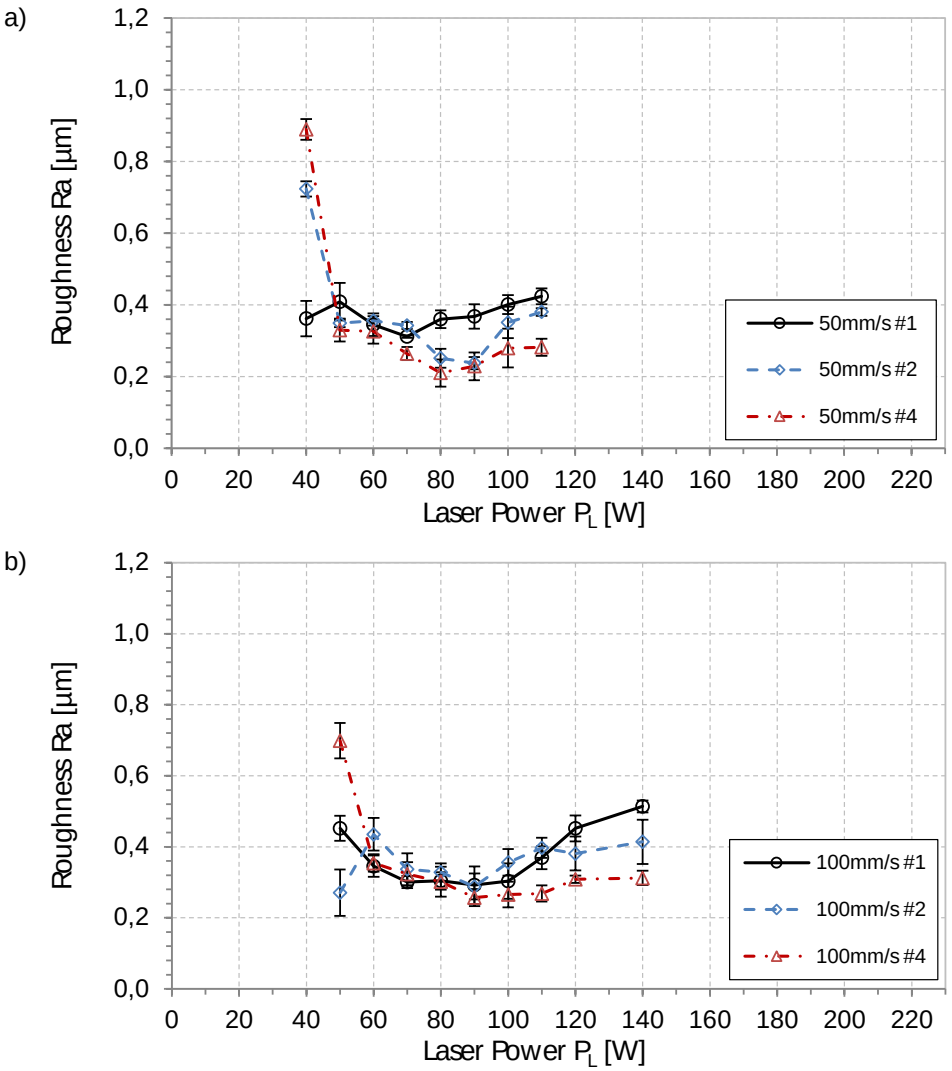

Figure 59:
Roughness Ra in dependence on laser power for different number of passes

Constant process parameters:
Tool: Q200_TD
dy = 40 µm
a) v_{scan} = 50 mm/s
b) v_{scan} = 100 mm/s

Figure 60:
Sa-spectrum in dependence on laser power

Constant process parameters:
Tool: Q200_TD
dy = 40 µm
v_{scan} = 50 mm/s
a) n = 1 pass
b) n = 2 passes
c) n = 4 passes

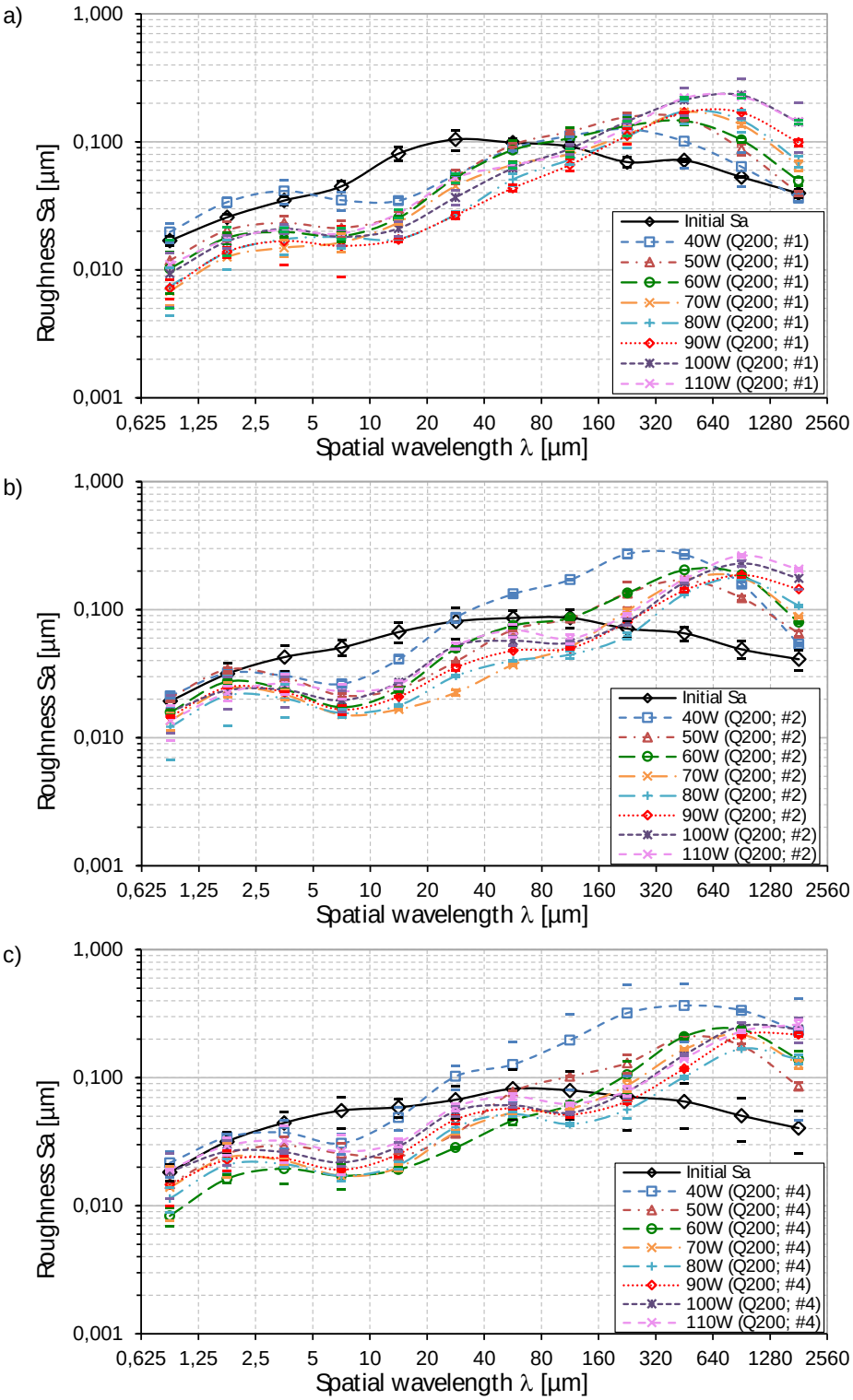

Figure 61:
Sa-spectrum in dependence on laser power

Constant process parameters:
Tool: Q200_TD
dy = 40 µm
v_{scan} = 100 mm/s
a) n = 1 pass
b) n = 2 passes
c) n = 4 passes

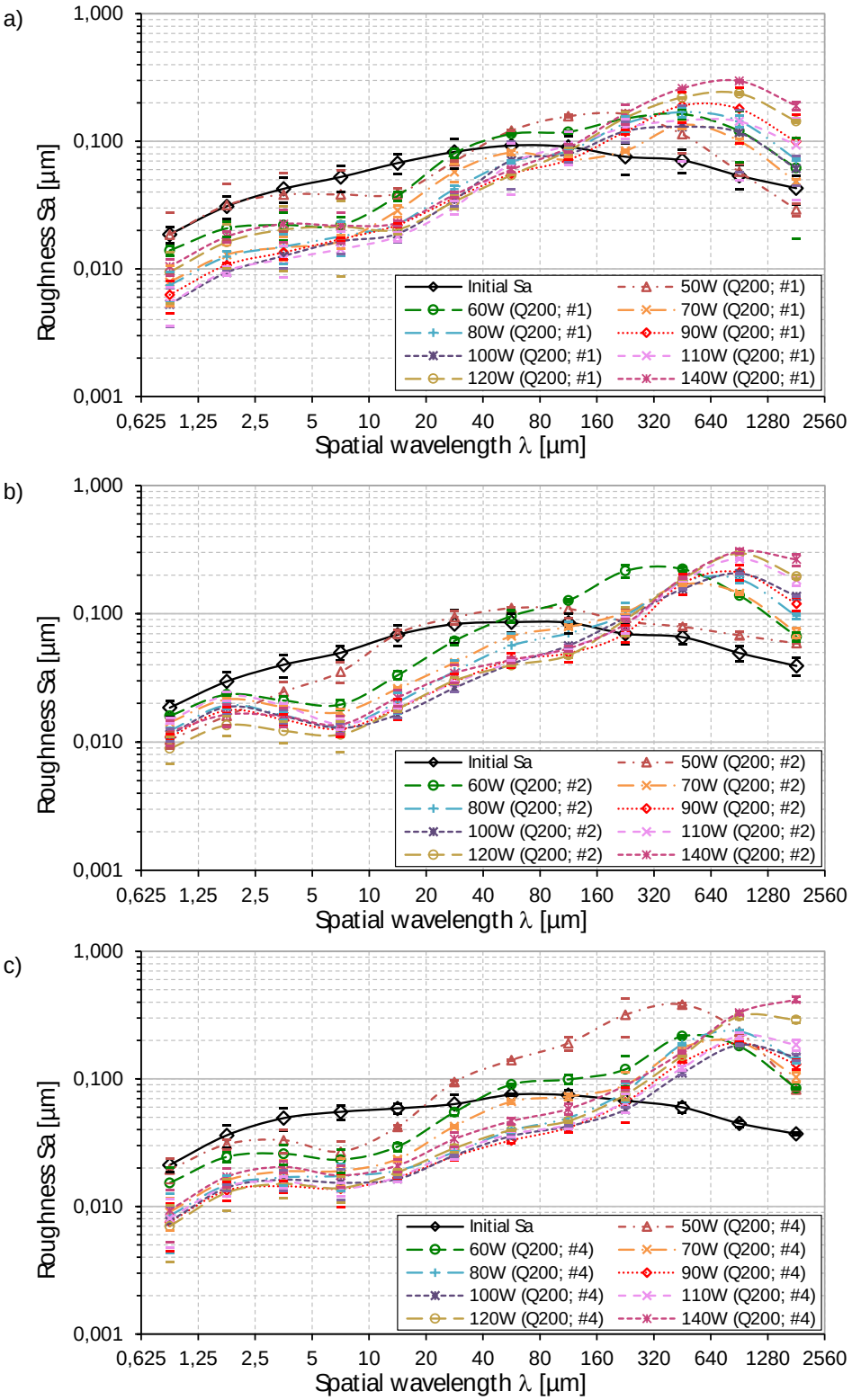

Figure 62:
Sa-spectrum in dependence on laser power

Constant process parameters:
Tool: Q200_TD
dy = 40 µm
v_{scan} = 200 mm/s
a) n = 1 pass
b) n = 4 passes

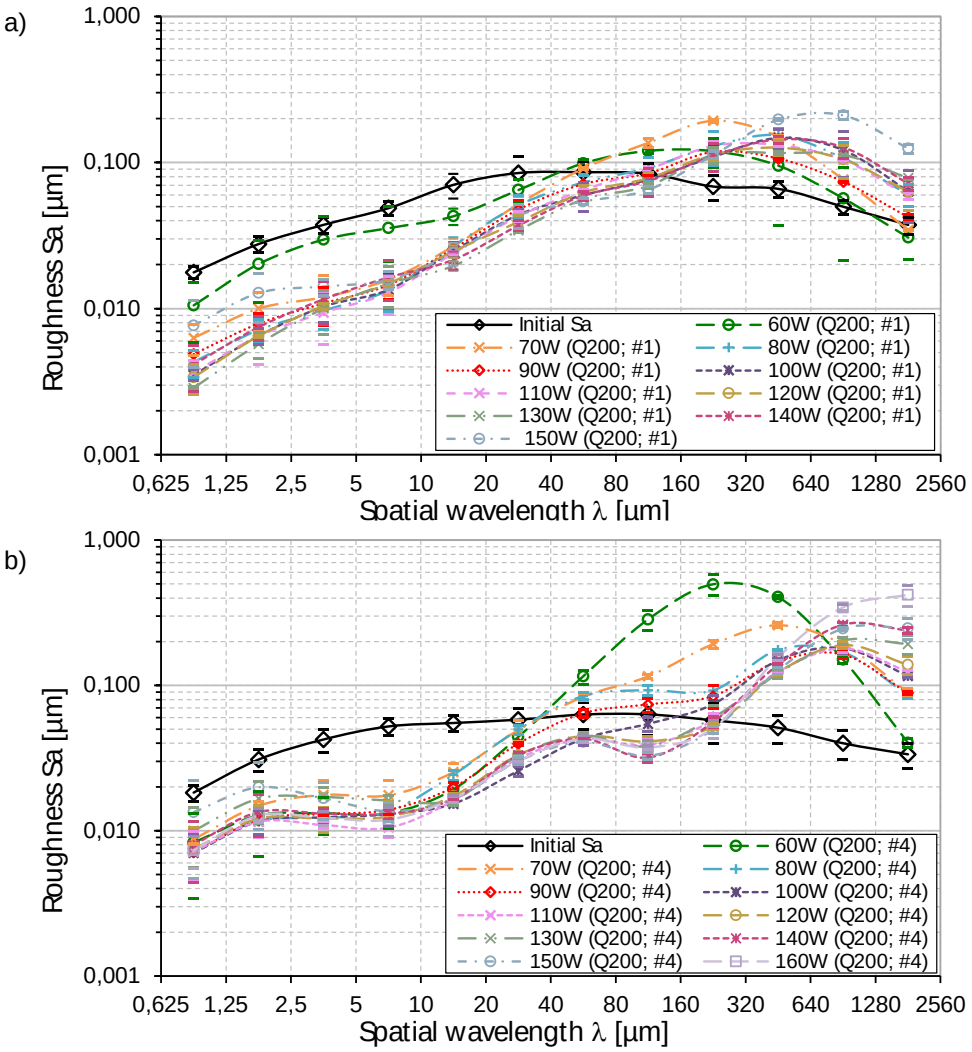

10.3 Micro polishing

Table 9.3.1: Employed energy per unit length and laser power for micro polishing

	Q100_TM			Q200_TM			Q400_TM		
Fluence [J/cm²]	[J/cm]	$P_{M\ SOLL}$ [W]	P_M [W]	[J/cm]	$P_{M\ SOLL}$ [W]	P_M [W]	[J/cm]	$P_{M\ SOLL}$ [W]	P_M [W]
3	0,3	6	5,9	0,6	24	23,6	1,2	96	93,4
4	0,4	8	7,9	0,8	32	31,0	1,6	128	126,6
5	0,5	10	9,7	1	40	38,7	2	160	159,3
6	0,6	12	11,8	1,2	48	46,8	2,4	192	189,8
7	0,7	14	13,7	1,4	56	55,8	2,8	224	219,6
8	0,8	16	15,5	1,6	64	63,3	3,2	256	251,6
9	0,9	18	17,7	1,8	72	71,4	3,6	288	286,8
10	1	20	19,8	2	80	79,2	4	320	315,8
11	1,1	22	21,8	2,2	88	86,7	4,4	352	348,9
12	1,2	24	23,7	2,4	96	94	4,8	384	382,7

10.4 Structuring by laser remelting

Figure 63:
Structure height in dependence on number of repetitions for different scan velocities

Constant process parameters:
Tool: Q200_TD
dy = 800 µm
a) λ = 1 mm
b) λ = 3 mm